Inelastic Proton Scattering from ^{138}Ba and ^{144}Sm and its Microscopic Interpretation*

Duane Larson,** Sam M. Austin, and B.H. Wildenthal

Cyclotron Laboratory and Department of Physics
Michigan State University, East Lansing, Michigan 48823

ABSTRACT

Differential cross sections for elastic and inelastic scattering of 30 MeV protons by ^{138}Ba and ^{144}Sm have been measured. The total resolution for the inelastic peaks was 7-10 keV FWHM, which permitted the observation of 20 excited states in ^{138}Ba and 18 states in ^{144}Sm below E_x=3.4 MeV, and determination of excitation energies accurate to 2 keV or less for these states. Based on characteristic shapes derived from angular distributions to states of known J^π, spin-parity assignments are made for the majority of the observed states. Collective model DWBA calculations were performed and deformation parameters extracted for all states of assigned J^π. Microscopic DWBA calculations which included the exchange amplitude were performed for the $2^+_{1,2}$, $4^+_{1,2}$, and $6^+_{1,2}$

---

* Research supported by the National Science Foundation.

** Present address: Neutron Physics Division, Oak Ridge National Laboratory, Oak Ridge, Tennessee 37830

states in both nuclei, using large-basis shell model wave functions to describe the nuclear states. These wave functions also provide an excellent description of the excited states in ^{138}Ba, and a good description of the energy levels in ^{144}Sm, as determined in our experiments. The two-body force used in the inelastic scattering calculations was obtained from a recent survey of inelastic scattering analyses. Polarization charges for the nucleons were extracted using the model of Atkinson and Madsen and were found to be essentially state and multipole independent. Two sets of shell model wave functions were employed for the ^{138}Ba calculation, and it was found that inelastic proton scattering clearly distinquished between the two sets, thus providing a sensitive test of the wave functions. Careful consideration of the transition densities derived from the wave functions permitted a direct study of properties of the wave functions.

I. INTRODUCTION

The recent interest in the N=82 nuclei stems from a number of sources. Foremost among these is the ~~observation~~ expectation that in a shell model picture, low-lying states in these nuclei are expected to be formed predominantly from proton configurations, the neutron shells being closed at 82 neutrons. Experimental evidence from proton[1,2] and neutron[3-5] transfer reactions confirms this expectation. Both proton stripping and pickup reactions on the N=82 nuclei populate only the $1g_{7/2}$, $2d_{5/2}$, $2d_{3/2}$, $3s_{1/2}$, and $1h_{11/2}$ single particle orbitals, thus indicating that proton orbitals other than these do not play a significant role in the wave functions for states of these nuclei. Neutron pickup reactions indicate that the orbitals above the last filled neutron major shell are empty, and conversely, neutron stripping reactions populate only the orbitals above the closed major shell, thus indicating that neutron shells below this are filled. The picture of the N=82 nuclei which emerges from these experiments is that of an effectively closed 82 neutron-50 proton core, such that low-lying states are formed by couplings of various numbers of valence protons in the aforementioned orbitals.

The single-particle nature of these nuclei has been thoroughly studied with the proton and neutron transfer reactions ~~described previously.~~ just mentioned Isobaric analog resonance experiments[6] have been used to determine, among other things, the positions of the low-lying neutron particle-hole states in the region beginning about 4 MeV, which indicates the limit of viability of the previously described model. Electromagnetic-decay aspects of the N=82 nuclei have been

measured through (β,γ),[7,8] (n,γ),[9] $(n,n'\gamma)$,[10] $(\alpha,xn\gamma)$,[11] and (γ,γ')[12] studies. These studies have been useful in assigning precise energies, as well as often limiting the possible J^π assignments to a few values. The $(\alpha,xn\gamma)$ studies have led to the observation of a series of isomeric 6^+ states in the even-even N=82 isotones.

Charged particle inelastic scattering studies have been limited mainly to the observation of the strongly excited states. Early inelastic scattering experiments[13] determined the positions of the first collective 2^+ and 3^- states. The $(p,p'\gamma)$ and $(d,d'\gamma)$ reactions[14] on the even-even isotones were studied in an attempt to locate the positions of excited 0^+ states in these nuclei by observing the E0 conversion electrons emitted in the transition to the ground state. More recently, the reactions $^{139}La(\alpha,\alpha')$,[15] $^{140}Ce(\alpha,\alpha')$,[15] $^{141}Pr(\alpha,\alpha')$,[16] $^{138}Ba(\alpha,\alpha')$,[17] $^{144}Sm(\alpha,\alpha')$,[18] $^{144}Sm(p,p')$,[18,19] and $^{144}Sm(^3He,^3He')$[19] have been used to study the collective nature of the strongly excited states in these nuclei. The angular distributions obtained from the latter five reactions were analyzed with the standard collective model formalism[20] and from that work J^π assignments were made, and deformation parameters β_L extracted. The ^{139}La and ^{140}Ce experiments were also analyzed with the collective model approach, and in addition, microscopic calculations were performed with a Gaussian two-body interaction and zero-order pseudo-spin orbit wave functions to describe the nuclear states. However, since alpha particles are strongly

absorbed near the surface of the nucleus, only the tails of the wave functions are important and this reaction is thus rather insensitive to many details of the wave functions.

In this paper we present results from inelastic proton scattering experiments performed at a bombarding energy of 30 MeV on ^{138}Ba and ^{144}Sm. Use of the high resolution system developed by Blosser, et al.[21] resulted in a total energy resolution for the inelastic peaks of typically 7-10 keV FWHM. Excitation energies accurate to within 1 to 2 keV were extracted and found to be in good agreement with those obtained in other high resolution experiments. Using empirical characteristic shapes derived from angular distributions to known states, spins and parities were assigned to the majority of the observed states.

Most previous microscopic DWBA calculations for inelastic scattering have been restricted to regions of the periodic table where particle-hole[22,23] or simple shell-model wave functions[24,25] were adequate for the description of the nuclear states. A second aspect of this work, in addition to spectroscopy, was to attempt to determine whether large basis shell model wave functions can account for the results of (p,p') measurements on nuclei with several valence nucleons. To this end, we have modified the Oak Ridge-Rochester shell-model codes[26] to calculate the necessary structure amplitudes in a form convenient for DWBA calculations. Calculations were performed using two sets of shell-model wave functions[27,28] for the low-lying 2^+, 4^+, and 6^+ states of ^{138}Ba and ^{144}Sm. For ^{138}Ba we obtain a reasonably good description of the angular distribution shapes, although the experimental cross

sections are strongly enhanced by collective excitations from the core. Using a model developed by Atkinson and Madsen[29] and discussed by McManus[30] for calculating the enhancement factor, we determined polarization charges appropriate to large basis shell model calculations in this mass region. Information on the structure of the wave functions was obtained from a detailed consideration of the shell model transition densities.

Preliminary reports describing part of this work have been published.[31,32]

In Section II we describe experimental aspects of this work; this is followed in Section III with individual discussions of all states observed up to E_x=3.3 MeV, and assignments of excitation energies and spin-parities where this was possible. In Sec. IV we discuss the shell model calculations which we use in this work, and Sec. V presents the optical model parameters we obtained from our elastic scattering data. Section VI outlines the relevant aspects of the DWBA theory used to describe the inelastic angular distributions, and lastly Sec. VII is a discussion of the results of this experiment.

II. EXPERIMENTAL

A. Proton Beam and Particle Detection

The measurements were made with 30 MeV protons from the Michigan State University sector-focussed cyclotron. An Enge split-pole spectrograph was used to analyze the scattered particles.

The amount of beam on target was monitored both with a current integrator in conjunction with a Faraday cup, and with a 5 mm thick silicon detector placed at 60° with respect to the incident beam. A set of removable slits located immediately prior to the spectrograph scattering chamber was used periodically to check the position of the beam on target. The typical size of the beam spot was 2 mm high by 4-5 mm wide. The entrance aperture of the spectrograph was 2° wide by 1.6° high, corresponding to a solid angle of 0.98 msr. During data accumulation this entrance aperture was the only slit between the cyclotron and the focal plane of the spectrograph. The energies of the proton beams were obtained from the calibration of the beam transport system magnets with an uncertainty of $\pm$0.1%. The beam energies for this experiment were 29.8 MeV for ^{138}Ba and 29.9 MeV for ^{144}Sm.

Angular distributions for elastic scattering and for scattering from the strong first 2^+ and 3^- states in both nuclei were measured using a 300 micron thick solid state position sensitive detector mounted at the focal plane of the spectrograph.[33] Signals proportional to E, the total energy loss of the particles passing through the detector, and xE, where x is the position along the detector, were analyzed for the type of particle and its location along the detector using a two dimensional data taking program.[34] The xE signal was digitally divided by the E signal, and energy vs. position spectra were displayed on a storage scope, where suitable lines were drawn defining the proton band. The computer then

identified all events falling between the lines as proton events and stored them in a position spectrum. The resolution obtained with the position sensitive detector was typically 30 keV FWHM. Its charge collection efficiency was mapped by gridding the peak from the elastically scattered particles across its surface in 3 mm steps. During data accumulation, the particles to be detected were positioned in a region which had been determined to have uniform efficiency.

The remainder of the inelastic scattering data were taken with Kodak NTB 25 or 50 micron nuclear emulsions placed in the focal plane of the spectrograph. Aluminum absorbers were used to stop all particles of greater stopping power than protons. Emulsions were exposed every 5° between 20° and 80° for ^{138}Ba and between 12° and 95° for ^{144}Sm. Two exposures were made at each angle, a short exposure to obtain data from the first 2^+ and 3^- states (for normalization purposes), and a sufficiently long exposure to obtain data with good statistics for most of the remaining states. The agreement between the position sensitive detector data and the emulsion data for the 2^+ and 3^- states was within statistics, so the data were averaged to obtain angular distributions for these states.

B. Preparation of Targets

Isotopically enriched compounds of $Ba(NO_3)_2$ (99.8%) and Sm_2O_3 (95.1%) obtained from Oak Ridge National Laboratory were used in the fabrication of the targets. The compound was placed in a Zr boat and heated in vacuum, causing reduction of the compound to the enriched metal and simultaneous evaporation of the

metal onto the target backing, which consisted of a 20 $\mu g/cm^2$ carbon foil plus a 3-5 $\mu g/cm^2$ layer of formvar supporting the carbon. The target material was evaporated over a surface 5/8" in diameter and appeared to be quite uniform. Typical target thicknesses ranged between 50 and 300 $\mu g/cm^2$. The targets were stored and transferred under vacuum to reduce oxidation, since in air complete oxidation occurred in only a few seconds for a thin ^{138}Ba target, and a few minutes for a ^{144}Sm target. Target thickness was estimated by comparing the measured elastic scattering to optical model predictions for the scattering.

The observed contaminants in the targets were carbon, oxygen, magnesium, and silicon, as determined from analysis of the inelastic scattering spectrum.

C. High Resolution System

The emulsion data were all taken using the high resolution system developed by Blosser, et al.[21] This system relies on dispersion matching,[35] kinematic compensation, and a feedback system which compensates for possible drift of any magnets in the cyclotron-beam transport system. In a dispersion-matched system, the line width of the scattered particles at the focal plane of the spectrograph is nearly independent of the energy spread of the incident beam. This is accomplished by using the focussing and dispersive elements of the beam transport system to adjust the dispersion of the beam on target to match the dispersion of the spectrograph. Kinematic compensation corrects for the change

in energy of the scattered particles across the finite entrance slit width, which arises from recoil of the target nucleus. This is accomplished by shifting the kinematic focal plane from its zero-order position (position for scattering from an infinitely heavy target nucleus). The approximate beam transport quadrupole settings for dispersion matching and correct position of the focal plane for kinematic compensation are calculated for a given reaction via a computer code.[36] Final minimization of the line width of the scattered protons is accomplished by using a stepped slit and detector device located at the focal plane of the spectrograph and illustrated in Fig. 1. The output of the solid state detector consists of three peaks, the high energy peak corresponding to protons transmitted through the slit, and the medium and low energy peaks corresponding to protons passing through the thin and thick jaws of the slit respectively. Fractional transmission of the elastically scattered protons through the 4 mil wide slit is maximized (thus minimizing the line width) by adjusting the dispersive elements of the beam transport system and other parameters of the experimental setup to maximize the intensity of the high energy peak. After minimization of the line width, this device serves as part of a computer controlled feedback system, which adjusts the spectrograph magnetic field to keep the elastically scattered protons centered on the transmission slit. This insures that the scattered protons remain at fixed points on the focal plane, independent of drifts in the system. Using this system we routinely obtained

resolutions of 7-10 keV FWHM at 30 MeV incident proton energy for the inelastically scattered particles. Figure 2 shows a spectrum obtained from ^{138}Ba at a laboratory angle of 35°, and Fig. 3 shows a spectrum from ^{144}Sm obtained at 40°. Typical beam currents on target were 100 na for ^{138}Ba (target limited) and 900 na for ^{144}Sm.

III. EXPERIMENTAL RESULTS

A. Energies of States in ^{138}Ba and ^{144}Sm

The techniques described in the previous section, in conjunction with nuclear emulsions, were used to obtain precise energies for the 20 excited states in ^{138}Ba and 18 states in ^{144}Sm which lie below E_x=3.4 MeV.

Peak centroids and intensities were extracted from the spectra obtained from the scanned emulsions at each angle. This was done with an automatic peak-fitting program, which aided in removing ambiguities in the background subtraction, in subtracting the broad impurity peaks and which afforded a consistent method of separating members of close lying doublets. The final adjustments to the basic energy calibration of the spectrograph were determined by fitting certain strong, isolated peaks in our (p,p') spectra to excitation energies previously determined for these levels by Ge(Li) spectrometer studies of gamma rays emitted in (β,γ) experiments. These calibration energies, along with their errors, are noted in Table I. This calibration of the spectrograph was then

used for interpolation and extrapolation to other excitation energies. These results enabled us to assign an excitation energy to each observed peak at each angle, provided the peak was not obscured by a contaminant. The extracted energies were averaged over all angles of observation, and the mean error in the centroid was calculated. The energies we have assigned to levels in ^{138}Ba and ^{144}Sm, along with the combined random and systematic errors, are listed in Table I. These energies are in excellent agreement with energies from (β,γ)[7,8] work on ^{138}Ba and $(\alpha,2n\gamma)$[11] work on ^{144}Sm.

B. Angular Distributions

Angular distributions have been measured for 18 of the 20 states observed in ^{138}Ba and 15 of the 18 observed states in ^{144}Sm, and for elastic scattering from both nuclei.

The elastic scattering angular distributions from ^{138}Ba and ^{144}Sm are shown in Fig. 4. The curves through the data are optical model calculations using the parameters of Becchetti and Greenlees.[37] The elastic scattering angular distribution data were normalized to the optical model calculations to obtain absolute normalizations. A comparison with calculations using other sets of optical model parameters[38] results in an estimate of 10% uncertainty in the absolute magnitude of the experimental cross sections. Relative uncertainties in our (p,p') cross sections arising from scanning errors, monitoring errors and statistical errors are typically 7%.

In order to obtain spins and parities from the measured angular distributions in a model independent fashion, empirical characteristic shapes were derived for 2^+, 3^-, 4^+, and 6^+ angular distributions in the following way. Examination of angular distributions for the known 2^+ states in both ^{138}Ba and ^{144}Sm revealed that they all had essentially the same shape. Using this fact, one average 2^+ shape was obtained from all of the known 2^+ distributions in both nuclei. This characertistic 2^+ shape was then used as a standard and compared to angular distributions for states of unknown J^π. Identical techniques were applied to the angular distributions of all assigned 3^-, 4^+, and 6^+ states in these nuclei to obtain 3^-, 4^+, and 6^+ characteristic shapes. The resulting empirical characteristic shapes for 2^+, 3^-, 4^+, and 6^+ angular distributions are compared in Fig. 5. We emphasize that the characteristic shape for a given J^π is an average of angular distribution data for all known states of that J^π from <u>both</u> nuclei. The states used in the determination of the empirical shapes are noted in Table I. The angular distribution data, along with the characteristic shape of the appropriate J^π which best approximates the data, are shown in Figs. 6 through 11. The remaining states, whose angular distributions are not similar to any of the characteristic shapes, are shown in Figs. 12 and 13. They may be grouped into two classes; either they are very weakly excited in this reaction, or they peak farther out in angle than the 6^+ states, implying they may be high spin states.

As explained in Sec. VIB5, direct DWBA theory would predict L-transfers of 2, 3, 4, and 6 for transitions from a 0^+ ground state to states with $J^\pi=2^+$, 3^-, 4^+, and 6^+, respectively. There are sufficient differences between the characteristic shapes, as seen in Fig. 5, to allow us to uniquely assign an L-transfer of 2, 3, 4, or 6 to the majority of the observed transitions. This in turn leads to assignments of $J^\pi=L$, with parity $(-)^L$, if it is assumed that non-normal parity states are weakly excited. In Sec. VIB5 we discuss the evidence which indicates that this assumption is valid. For example, an angular distribution for a state of unknown J^π which matches the 4^+ characteristic shape has an L-transfer of 4. This in turn leads to a J^π assignment of 4^+, and not the non-normal parity 3^+ or 5^+, as direct DWBA theory would also allow.

Our assignments for the spin and parity of excited states we observe in ^{138}Ba and ^{144}Sm, based on the agreement of the measured angular distributions with the empirical characteristic shapes, are given in Table I.

C. Discussion of States in ^{138}Ba

To organize the discussion of our experimental results, it is convenient to divide the levels which we observe into groups, each group being identified by its J^π assignment.

1. 2^+ States (Figure 6)

The states at 1436, 2218, 2639, 3339, and 3368 keV are all in good agreement with the 2^+ characteristic shape; we thus assign $J^\pi=2^+$ to these states. The state at 1436 keV is firmly established as 2^+ from Coulomb excitation,[39] conversion coefficient,[40] and

(α,α') inelastic scattering measurements.[17] The state at 2218 keV is observed to have a strong decay branch to the ground state in neutron capture[9] and (β,γ)[7,8,40] decay experiments. This limits the spin to 1 or 2. Achterberg, et al.[40] assign positive parity to this state from conversion coefficient measurements. Thus our assignment of $J^\pi=2^+$ is consistent with previous data. The level at 2639 keV, observed in (n,γ)[9] and (β,γ)[7,8] studies, also has a strong decay branch to the ground state, thus limiting its spin to J=1, 2. However, a log ft value of 7.4 for β decay from the $J^\pi=3^-$ state of ^{138}Cs given by Carraz, et al.[8] eliminates J=1. The two levels at 3339 and 3368 keV also decay directly to the ground state, limiting their spins to J=1,2. Angular distributions from (α,α') studies[17] also suggest an assignment of $J^\pi=2^+$ for these states. The angular distribution for the state we observe at 3050 keV is not in agreement with the 2^+ characteristic shape at forward angles, thus we leave it unassigned. Hill and Fuller[7] assign J=1, 2 to this state.

2. 3^- States (Figure 8)

The only 3^- state we observe in ^{138}Ba is the one previously assigned[13,17] at 2881 keV. It is the strongest state in the (p,p') spectrum, and is strongly populated in (d,d')[14] and (α,α')[17] experiments and in (n,γ)[9] studies, where it decays strongly to the 2^+ state at 1436 keV.

3. 4^+ States (Figure 9)

The states at 1898, 2308, 2584, 2779, and 3156 keV have angular distributions which are in good agreement with the characteristic 4^+ shape; we assign $J^\pi=4^+$ to these states. The level at 1898 keV is established as 4^+ from (α,α')[17] angular distributions, $(d,{}^3He)$[2] measurements which suggest an assignment of 4^+ or 6^+, and conversion coefficient[40] studies which, when combined with the $(d,{}^3He)$ work, limit the spin to 4^+.

The state at 2308 keV is assigned $J^\pi=3^+$, 4^+ from conversion coefficient studies of Achterberg, et al.[40] A J=3, 4 assignment has also been suggested by (n,γ)[9] and (β,γ)[7] studies based on the strong decay to both the first 2^+ and 4^+ states. Since non-normal parity states such as 3^+ are very weakly excited in inelastic scattering on heavy nuclei, we assign $J^\pi=4^+$ to this state, which is also the suggested assignment from (α,α')[17] studies.

Hill and Fuller[7] and Mariscotti, et al.[9] observe a state in the vincity of the state we see at 2584 keV. Hill and Fuller limit the spin of this state to J=1, 2 on the basis of a gamma ray branch to the ground state. However, the angular distribution we measure has a 4^+ shape. Thus, we believe there are two distinct levels in this vicinity since the state seen by Hill and Fuller is clearly not a 4^+ by virtue of the gamma ray to the ground state, and ours is not a J=1 or 2 by virtue of the angular distribution. It is informative to consider ratios of intensities of two gamma ray depopulating this level, as measured by Hill and Fuller in their

(β,γ) work and Mariscotti, et al. in their (n,γ) studies.

$$\frac{I(2583\rightarrow1436)}{I(2583\rightarrow0)} = \sim 7.8 \qquad (n,\gamma)$$

$$\frac{I(2583\rightarrow1436)}{I(2583\rightarrow0)} = \sim 2.3 \qquad (\beta,\gamma)$$

Thus $$\frac{(n,\gamma)}{(\beta,\gamma)} = \sim 3.3$$

Similar ratios for the 2583-2218 keV transition relative to the ground state transition are also in the ratio of ~3:1. The non-equality of the (n,γ) and (β,γ) ratios can be taken as an indication that the (n,γ) and (β,γ) experiments are populating two levels with different intensities in the vicinity of 2583 keV. In addition, Hill and Fuller see a broadening of the gamma ray line connecting their state at 2583 keV with the 2445 keV state. They attribute this to the decay of the 2445 keV to the 2307 keV state, but we suggest this could also be due to a state at 2584 keV decaying to the 2445 keV state. The broadened decay line they observe would then correspond not to two but to three different transitions. We will find in Sec. VIIA that the shell model predicts a 1^+-4^+ doublet near this energy, which would be in excellent agreement with experimental observation. A 1^+ state would decay to the ground state via an M1 transition, but since it is a non-normal parity state we would not expect to populate it strongly in (p,p'). The angular distribution we measure for this doublet would then assume the shape characteristic of the 4^+ member of the doublet.

The state at 2779 keV is observed in (β,γ),[7] but not (n,γ)[9] work and decays to both of the first excited 2^+ and 4^+ levels, thus limiting its spin to J=2, 3, 4. It may also correspond to the state at 2.79 MeV in $(d,^3He)$[2] experiments.

The state at 3156 keV which we observe is probably not the same state reported by Hill and Fuller[7] at 3164 keV, since the 8 keV difference in energies is well outside the combined errors. However, they assign spin limits of J=2, 3, 4 to their state based on its decay to the first excited 2^+ and 4^+ states. These two experiments are the only ones which report a state near this energy.

4. 6^+ States (Figure 11)

We assign $J^\pi=6^+$ to the state at 2090 keV, and a tentative (6^+) to the level at 2201 keV. Angular distributions for known 6^+ states are scarce in the literature. We have obtained an angular distribution for the state at 2090 keV, which has been assigned 6^+ by Carraz, et al.[8] on the basis of its measured half-life of 0.8 μsec. This assignment is consistent with systematics of 6^+ states in N=82 nuclei; isomeric 6^+ states have been identified[41] in all even-even isotones from ^{134}Te to ^{146}Gd. A 6^+ assignment is also consistent with the absence of this state in the (n,γ)[9] work, and its negligible feeding in the β decay of the 3^- ground state of ^{138}Cs.

The state at 2201 keV is the subject of some controversy. Carraz et al.[8] propose that this state has $J^\pi=(5^-)$, while Achterberg, et al.[40] propose $J^\pi=(4^+,5^+)$, based on the measurement

of log ft values from the decay of $^{138m,g}Cs$ and the assumption of $J^{\pi}=3^{-}$, (6^{-}) for the ground and isomeric states respectively of ^{138}Cs. This state is quite weak in our spectra, and not well resolved from the strong 2^{+} at 2218 keV. Our angular distribution for this state is not inconsistent with any of these tentative assignments. Both the 4^{+} and 6^{+} characteristic shapes are drawn through the angular distribution for this state in Fig. 11. We would favor a (6^{+}) assignment for this state, based on the predictions of shell model calculations, and to some extent, on the shape of the angular distribution.

5. Other States (Figure 12)

We make no J^{π} assignments for the states we observe at 2415, 2445, 3254, and 3285 keV. The transitions to these states are all very weak, the largest cross section at any angle being less than 10 μb/sr. Achterberg, et al.[40] have assigned $J^{\pi}=3^{+}$ to the state at 2445 keV, based on angular correlation and conversion-coefficient measurements. They also suggest a $J^{\pi}=5^{+}$ assignment for the state at 2415, based on log ft values of the β decay feeding it from $^{138m,g}Cs$. Our angular distributions for these states, by virtue of their magnitude, support non-normal parity assignments. The two remaining states at 3254 and 3285 keV are not seen in previous work on this nucleus, and our angular distributions do not shed any light on possible J^{π} assignments for them. The 2929 and 2990 keV states which were observed only at 20 degrees are very weak ($\sigma(20°)<1$ μb/sr) and are therefore not likely to be low spin normal

parity states. Hill and Fuller[7] suggest spins of J=1, 2 and 1, 2, 3, 4, respectively for these states.

D. Discussion of States in ^{144}Sm

1. 2^+ States (Figure 7)

We assign $J^\pi=2^+$ to the states at 1661, 2423, and 2800 keV. The 1661 keV level is the first excited state in ^{144}Sm; its J^π is firmly established from Coulomb excitation,[42] (β,γ)[43] studies and (α,α') and (p,p')[18] experiments. Barker and Hiebert[18] observe a 2^+ state at 2.45 ± 0.2 MeV via (p,p') and (α,α') reactions, which we assume corresponds to our level at 2423 keV. The state at 2800 keV has been assigned $J^\pi=2^+$, from comparison of its angular distribution with the 2^+ characteristic shape. It has also been observed weakly in the β^+ decay[43] of the 1^+ ground state of ^{144}Eu.

2. 3^- States (Figure 8)

We assign $J=3^-$ to the states at 1811 and 3227 keV. The state at 1811 keV is well established to have $J^\pi=3^-$ from (α,α') and (p,p') experiments,[18] and is the strongest state observed in our ^{144}Sm spectra. The angular distribution of the previously unobserved state at 3227 keV is very similar to that of the 1811 keV state, as well as to the angular distribution for the collective 3^- state in ^{138}Ba. On this basis we assign the 3227 keV state $J^\pi=3^-$.

3. 4^+ States (Figure 10)

We assign $J^\pi=4^+$ to the states at 2191, 2588, 2883, and 3020 keV on the basis of agreement of their angular distributions with the 4^+ characteristic shape. The level at 2191 keV has previously been assigned $J^\pi=4^+$ on the basis of gamma ray systematics,[41] and recent (α,α') and (p,p') experiments[18] verify this assignment. We assume that this is the level at $2.21\pm.02$ MeV observed in (d,d') and (p,p') studies.[14] The states at 2588, 2883, and 3020 keV have not been previously reported. They are in good agreement with the characteristic 4^+ shape, with the possible exception of the 3020 keV state, which falls off somewhat too rapidly for angles larger than 50°. These 4^+ assignments are consistent with the fact that Kownacki, et al.[11] have not observed these states in the $^{142}Nd(\alpha,2n)^{144}Sm$ reaction which preferentially populates states with $J\geq 8$. Studies of the β decay of the ^{144}Eu 1^+ ground state[43] also show no evidence for levels at these energies, which is in agreement with our 4^+ assignments since population of 4^+ states via this decay would be unique second forbidden.

4. 6^+ States (Figure 11)

The Stockholm group[41] has assigned the state at 2324 keV a spin-parity of 6^+, based on its life-time of 0.88 μsec. This agrees with systematics of 6^+ states in the N=82 nuclei. However, our angular distribution for this state is only in qualitative agreement with the characteristic 6^+ shape due to the rise of the data at forward angles. This could be due to a very close-lying

low spin state which would cause the experimental angular distribution to rise at forward angles. This possibility is supported by the fact that the FWHM of this peak is consistently 10-15% larger than that of other nearby peaks. We also assign $J^{\pi}=6^{+}$ to the previously unobserved state at 3308 keV on the basis of the shape of its angular distribution.

5. Other States (Figure 13)

We make no J^{π} assignments for the states we observe at 2826, 3123, 3196, and 3266 keV. The state at 3123 keV has been assigned $7^{(+)}$ by the Stockholm group[11] in their search for high spin states using the $^{142}Nd(\alpha,2n\gamma)^{144}Sm$ reaction and coincidence techniques. Our angular distribution for this state is consistent with a high spin state; if this is the same state seen by the Stockholm group, we would favor a 7^{-} rather than 7^{+} assignment as it is fairly strongly excited. The angular distributions for the levels at 2826 and 3196 keV peak far out in angle, suggestive of high spin states, but the Stockholm group does not place any levels at these energies. The 2800 (2^{+}) and 2826 keV levels are seen as a doublet in the (α,α') and (p,p') work of Barker and Hiebert.[18] We also note the similarity of the 3123 and 3196 keV angular distributions, which leads one to doubt that they are both doublets. The state at 3266 keV has not been observed previously, and is excited very weakly in the present experiment. The angular distribution for this state does not allow us to make any suggestions for its spin and parity.

IV. N=82 WAVE FUNCTIONS

A. Conventional Shell Model

As discussed in the Introduction, we have used large basis shell-model wave functions to describe the nuclear states involved in the present experiment. This section describes the details of the conventional shell model calculation[27,28] which was done with the Oak Ridge-Rochester shell model code.[26]

The basis space for the shell-model wave functions consists of the $1g_{7/2}$ and $2d_{5/2}$ orbits, plus one-proton excitations from this subspace into the $3s_{1/2}$ or $2d_{3/2}$ orbits. The two-body interaction between the valence nucleons was parameterized in terms of a modified surface delta interaction (MSDI), with the four single particle energies and the two MSDI parameters fixed by fitting to binding energies and energy levels of known J^{π} in the N=82 nuclei.

Two Hamiltonians were used. The MSDI parameters for the first Hamiltonian were obtained by fitting to levels of known J^{π} in N=82 nuclei from ^{136}Xe through ^{145}Eu (A=136-145), while those for the second Hamiltonian were obtained by fitting to levels from ^{136}Xe through ^{140}Ce (A=136-140). The A=136-145 interaction was applicable to both ^{138}Ba and ^{144}Sm, while A=136-140 was designed for the lower mass N=82 isotones, and hence was used only for ^{138}Ba. Thus two sets of wave functions were calculated for ^{138}Ba, but only one set for ^{144}Sm. The basis space was the same for all calculations; only the parameters of the Hamiltonian differed.

The basic difference between the two Hamiltonians is the $g_{7/2}$-$d_{5/2}$ single particle energy splitting, which increased from about 500 keV for the A=136-145 interaction to about 900 keV for the A=136-140 interaction. Table II lists the single particle energies and MSDI parameters for both interactions. It is found that the eigenvalues and eigenvectors calculated with the A=136-140 interaction yield better agreement with experimentally known spectra, pickup and stripping spectroscopic factors and electromagnetic data for the lower N=82 isotones than do those calculated with the A=136-145 interaction. In particular, the A=136-140 calculations are in excellent agreement[28] with recent data on ^{133}Sb and ^{134}Te, the one and two proton N=82 isotones, although levels from these nuclei were not included in the search procedure which fixed the parameters of the Hamiltonian. It is reasonable that the A=136-145 Hamiltonian might give poorer results for the lighter N=82 isotones. For the upper N=82 isotones, the effects of the limited basis space appear to be important. For example ^{144}Sm, which has 12 valence protons, effectively has a basis space consisting of two holes in the $g_{7/2}$-$d_{5/2}$ orbits and one-particle excitations out of these orbits. The physical low-lying states of ^{144}Sm presumably have substantial amplitudes in their wave functions for configurations outside of the allowed basis space, such as $(1h_{11/2})^2$, $(2d_{3/2})^2$, and $(3s_{1/2})^2$. Including these states in the searching procedure which determines the parameters of the A=136-145 Hamiltonian could well distort the parameters to compensate for components outside of the basis space. This would in turn

decrease the accuracy of the calculations in the lower isotones. In light of this, the superiority of results calculated for ^{138}Ba with the A=136-140 interaction over those calculated with the A=136-145 interaction is expected. Moreover, it is expected that the best results calculated for ^{138}Ba should be superior to the best for ^{144}Sm, since the basis space is physically more realistic for A≤140. We have used both the A=136-140 and A=136-145 sets of wave functions in the DWBA calculations for ^{138}Ba, to see if inelastic proton scattering can identify one set of wave functions as definitively better than the other. Only the A=136-145 interaction was used in the ^{144}Sm calculation, as previously noted. With the basis space used in this calculation, states in ^{138}Ba have between 50 and 220 components in their wave functions, while states in ^{144}Sm have between 10 and 45 components. In the following discussion we use the notation J_i^π, where i refers to the first or second excited state of spin and parity J^π.

B. Other Structure Calculations

Properties of the N=82 nuclei have also been calculated by methods other than the conventional shell model approach of Wildenthal.[27] Rho[44] performed a two-quasiparticle calculation for the even N=82 nuclei, employing a Gaussian form as the residual nucleon-nucleon interaction. At the time of that work, the single particle energies needed in the calculation were not experimentally known. The results of this calculation are in qualitative agreement with experiment, but no 0^+ or 6^+ levels

were calculated. In a later calculation, Waroquier and Hyde[45] used an approach similar to Rho, but employed the inverse gap equation technique[46] to obtain the single particle energies for their calculation. In addition they calculated the 0^+ and 6^+ states and in general obtained good agreement with existing data. Comparisons of their calculated energy levels and those of the conventional shell model which we use in this work are given in Ref. 45.

A new coupling scheme, developed by Hecht and Adler,[47] and employed by Baker and Tickle,[15] Baer, et al.[16] and Jones, et al.[2] in their work on N=82 nuclei, predicts energy levels in good agreement with our experimental results for ^{138}Ba. Calculations performed[2] with this coupling scheme and using a basis space very similar to that of Wildenthal result in wave functions with at most 23 components. It is encouraging that this scheme, with its apparent simplicity, is able to reproduce the salient features of the conventional shell-model which we have employed in this work. A comparison of the energy levels predicted by the pseudo spin-orbit scheme and the conventional shell model are given for ^{138}Ba in Ref. 2. This coupling scheme also predicts approximate selection rules for relative strengths of excited states observed in inelastic scattering. This will be discussed further in Sec. VIB5.

V. OPTICAL MODEL

Essential ingredients in any DWBA calculation are the optical model parameters which describe the elastic scattering in the entrance

and exit channels. A number of optical model parameter studies[37,38,48] have been made for 30 MeV protons incident on nuclei with A between 40 and 208. From these studies, formulae result which allow one to interpolate the "best fit" parameters to nuclei and energies other than those specifically used in the studies. However, there is a large gap from tin (A~120) to lead (A=208) for which very little precise elastic scattering data exists, and thus no information for this region was included in the optical model studies. It was not clear, therefore, that the parameters which these studies predict would properly account for the elastic scattering from ^{138}Ba and ^{144}Sm.

Fortunately, parameters predicted by two previous studies[37,38] yielded results which are in very good agreement with our elastic scattering data. The optical model parameters of Becchetti and Greenlees[37] predict an elastic scattering angular distribution for ^{138}Ba(^{144}Sm) which results in a chi square per point between theory and experiment of 3.4 (5.3), while Set II (Set I) from Satchler's analysis[38] yields a fit with a chi square per point of 4.0 (4.3). As discussed previously in Sec. IIIB, these excellent theoretical fits allowed us to normalize our elastic angular distribution data to theory in order to obtain absolute cross sections for the inelastic scattering data. After this normalization was determined, the predicted parameters were allowed to vary in a search to obtain the optimum parameters for use in the DWBA calculations.

The optical model potential used in our analysis has the usual form

$$V(r) = -V_R(1+e^{X_R})^{-1} - i(W_{vol}-4W_{surf}\frac{d}{dx_{IM}})(1+e^{X_{IM}})^{-1}$$

$$+ (\frac{\hbar}{m_\pi c})^2 V_{LS}\frac{1}{r}\frac{d}{dr}(1+e^{X_{LS}})^{-1} \qquad \text{(Eq. 1)}$$

where $X_R = (r-r_R A^{1/3})/a_R$

$X_{IM} = (r-r_{IM}A^{1/3})/a_{IM}$

$X_{LS} = (r-r_{LS}A^{1/3})/a_{LS}$.

The Coulomb potential is that of a uniformly charged sphere with radius $r_c A^{1/3}$.

To obtain an optimum set of optical model parameters three different sets were utilized as starting parameters for the searching procedure. They are (1) the set predicted from the global optical model analysis by Becchetti and Greenlees,[37] (2) Set I, and (3) Set II from the work of Satchler[38] on 30 MeV proton elastic scattering.

The final best fit parameters for each set are presented in Table III. The final values are all within 5% of the starting values, with the exception of the surface absorption strength in Satchler, Set I, which decreases by 15% for ^{138}Ba. The elastic angular distributions calculated with the three sets of parameters and normalized to the data differed by less than seven percent at any angle and differences were indistinguishable on the scale of Fig. 4. The total DWBA cross sections for the first 2^+, 4^+, and

6^+ states in ^{138}Ba calculated with each set of parameters are also given in Table III. These give an indication of the sensitivity of the DWBA calculations to changes in optical model parameters. The ratios of the cross sections for J=2, 4 and 6 are essentially constant; hence the main difference between the various sets is an overall normalization which is at most 10%. For the calculations presented in this paper, Set SII in Table III was chosen for ^{138}Ba as it gave the smallest chi square per point, and resulted in total cross sections intermediate in value between BG and SI. The ^{144}Sm calculations were done with Set SI.

VI. DISTORTED WAVE BORN APPROXIMATION (DWBA) THEORY

A. Collective Model DWBA

We have performed conventional collective model[20] DWBA calculations, deforming both the real and imaginary terms of the optical model potential, corresponding to all of the transitions we observe. This type of analysis has been thoroughly studied for 30 MeV (p,p') reactions.[49] We have extracted deformation parameters β_L' for all states which have been assigned a J^π value by normalizing the calculated angular distribution to the measured distribution using a chi-squared fitting program,[50] and emphasizing the forward angle data. The resulting β_L' values may be used to estimate the strength of the corresponding B(EL) transition between

the ground state and the state of interest. The formalism of Bernstein[51] has been designed to describe the extraction of isoscalar transition rates from inelastic α scattering. However, the method can be applied to our results if one assumes (1) that spin and isospin flip amplitudes are small, and (2) the contribution from the interior of the nucleus, which contributes to proton but not alpha inelastic scattering, can be neglected. There is some evidence that these are reasonable assumptions, since deformation lengths $\delta'=\beta'R'$ obtained from inelastic proton and alpha scattering are often in good agreement.[18,51] However, in the microscopic description discussed in the next section, we explicitly take account of the fact that the proton projectile interacts more strongly with the neutrons of the target than with the protons. This implies that the deformation parameters β_L' extracted from (p,p') and (α,α') reactions should be different. Since this does not appear to be the case, these differences must somehow be absorbed in the parameterization of the optical potential. The most accurate comparisons can be obtained for the relative strengths for a fixed L transfer in a limited mass region, since theoretical and experimental errors will tend to cancel out. In this case, the B(EL) values which this method of analysis yields will be useful as a guideline for comparison to B(EL) values predicted by nuclear structure models, such as the shell model. The isoscalar transition rates are calculated (in single particle units) from the equation[51]

$$G_L = \frac{(Z\beta_m)^2(3+L)^2}{4\pi(2L+1)} \qquad \text{(Eq. 2)}$$

where β_m, the mass deformation parameter, is obtained from the prescription of Bernstein[51]

$$\beta' R' = \beta_m R_m \qquad \text{(Eq. 3)}$$

where β' is obtained from the relation $\frac{\sigma_{expt}}{\sigma_{thy}} = (\beta')^2$.

R' is the imaginary radius obtained from optical model fits to elastic scattering, and $R_m = 1.2\ A^{1/3}$, the cutoff radius for a uniform charge density model of the nucleus. The results for G_L for a more realistic Fermi charge distribution can be obtained by multiplying the result from Eq. 2 by a tabulated correction factor given in Ref. 51. The results of this analysis will be presented in Sec. VIIB.

B. Microscopic DWBA

1. Distorted Wave Calculations

The microscopic DWBA calculations were performed with the code DWBA70 written by Raynal and Schaeffer.[52] This code is based on the helicity formalism of Raynal[53] which automatically accounts for all values of orbital angular momentum L and spin angular momentum S that can be transferred in a given transition from a $J^\pi = 0^+$ ground state. The knock-on exchange term, which describes exchange between the projectile and target valence nucleons, is included in the scattering amplitude. Central, tensor and

spin-orbit interactions can be included in the two-body force between the projectile and target nucleon.

The cross section is defined such that

$$\frac{d\sigma}{d\Omega} = \frac{1}{2} \sum_{\substack{\sigma_i \sigma_f \\ M}} f^*_{\sigma_f M,\sigma_i} f_{\sigma_f M,\sigma_i} \qquad \text{(Eq. 4)}$$

where

$$f_{\sigma_f M,\sigma_i} = -\frac{m}{2\pi\hbar^2} \sum_{j_h,j_p} Z(j_h j_p)^{JT} \langle \chi^{(-)}_{k_f \sigma_f} (j_p j_h) J\mu | v | \chi^{(+)}_{k_i \sigma_i} \rangle_A \qquad \text{(Eq. 5)}$$

1. σ_i, σ_f are the helicities of the incoming and outgoing particles, respectively, and f is the scattering amplitude for the transition.
2. M is the helicity of the residual nucleus.
3. $\underline{k}_i, \underline{k}_f$ are the momenta of the incoming and outgoing particles, respectively.
4. The subscript A refers to the antisymmetrized matrix element.

A target nucleus with spin zero ground state is assumed, and the final state of angular momentum J and isospin T is described by a particle in orbital j_p and a hole in orbital j_h. v is the two-body interaction between the projectile and target nucleons, and the $\chi^{\pm}$ are the distorted waves which describe the relative motion of the target and projectile.

The quantity $Z(j_h j_p^{JT})$ is the spectroscopic amplitude[54] for the transition and contains all of the nuclear structure information needed to describe the initial and final states of the target nucleus. A full description of the helicity formalism is given in Ref. 53.

2. Spectroscopic Amplitudes

The spectroscopic amplitudes $Z(j_h j_p^{JT})$ are of major interest in this paper. The procedures used to calculate these quantities depend upon the model used to describe the states of the target nucleus. In this work the target states are described by the large basis shell model wave functions described in Sec. IVA. We have modified the Oak Ridge-Rochester shell model codes[26] to calculate the spectroscopic amplitudes $Z(j_h j_p^{JT})$ in a form convenient for DWBA calculations. The LSJ coupling formalism, where L, S, J, are the transferred orbital, spin and total angular momentum, is used by most workers performing DWBA calculations, and is more familiar than the helicity formalism previously discussed. The following discussion will therefore be based on notation very similar to that of Satchler[24] and Petrovich.[55] For the direct term of the scattering amplitude, the spectroscopic amplitudes are related to the single particle matrix elements defined by Satchler.[24,25]

$$[M_L^T(j_p j_h)\delta_{S,0} + N_{L1J}^T(j_p j_h)\delta_{S,1}] \equiv M_{LSJ}^T(j_p j_h) = \frac{\sqrt{2}\,\hat{T}\,\hat{J}_i \hat{j}_p}{\hat{J}_f}$$

$$* \tfrac{1}{2}T\tau_a, \tau_b - \tau_a | \tfrac{1}{2}\tau_b > * Z(j_p j_h^{JT}) * \langle \ell_p j_p \tfrac{1}{2} || T_{LSJ}(\theta,\phi,\underline{\sigma})\underline{\tau} || \ell_h j_h \tfrac{1}{2} \rangle \qquad \text{(Eq. 6)}$$

where T_{LSJ} is the spin angle tensor, $\underline{\tau}$ is the isospin operator, J_i, J_f are the spins of the initial and final states in the target nucleus, and $\hat{x} \equiv \sqrt{2x+1}$.

3. Elements of the DWBA Formalism (Direct Amplitude)

The transition density can now be defined

$$F^{LSJ,T}_{(r_1)} = \sum_{j_p j_h} M^{T}_{LSJ}(j_p j_h) u_{n_p \ell_p}(r_1) u_{n_h \ell_h}(r_1) \qquad \text{(Eq. 7)}$$

where $u_{n\ell}(r)$ are the bound state radial wave functions of the active valence particles. We use harmonic oscillator wave functions for the bound states, with the oscillator parameter given by[56]

$$\hbar\omega = \frac{45}{A^{1/3}} - \frac{25}{A^{2/3}} \qquad \text{(Eq. 8)}$$

The form factor $G^{LSJ,T}_{(r_0)}$ for the direct term of the scattering amplitude is related to the transition density through the relation

$$G^{LSJ,T}_{(r_0)} = \int F^{LSJ,T}_{(r_1)} V^{ST}_{L}(r_0, r_1) r_1^2 \, dr_1 \qquad \text{(Eq. 9)}$$

where $V^{ST}_{L}(r_0, r_1)$ is the L^{th} multipole in the decomposition of the two-body force between the bound nucleon and the incident projectile. The form factor $G^{LSJ,T}_{(r_0)}$ thus contains all of the structure information which describes the states of the target nucleus, as well as the information concerning the form of the interaction between the projectile and target nucleon.

The form factor $G^{LSJ,T}_{(r_0)}$ is then folded in with the incident and exit channel optical model wave functions, and squared to get the direct contribution to the DWBA cross section. It is clear from the previous discussion that the magnitude and the shape of the angular distribution is dependent on (1) the optical model parameters which describe the elastic scattering from the target nucleus, (2) the form of the two-body force between the projectile and target nucleons, and (3) the transition density. We now consider these elements of the cross section in turn.

The procedure for determining the optical model parameters is well defined. The various parameters of the optical model are adjusted until one obtains the best fit to the measured elastic scattering from the target nucleus, as was discussed in Sec. V.

The form of the two-body force is, however, not well defined. The most desirable two-body force to use would be one which describes two-nucleon scattering, such as the Hamada-Johnston potential.[57] However, due to its hard core, this potential cannot be used in its original form. A common technique is to apply the Scott-Moszkowski separation method[58] to the attractive-even state components of the Hamada-Johnston potential, add second order effects due to the tensor interaction, and neglect the odd state parts on the basis that they are much weaker than the even state components. This results in an even state force similar to the Serber force. This approach, used by Love and Satchler,[25] results in a potential which retains the basic features of the original potential at low energies and is useable

in inelastic nucleon-nucleus scattering calculations as well as in bound state calculations. Petrovich, et al.[59] have used a similar approach with the Kallio-Kolltveit[60] interaction as the effective interaction and they find that this realistic force gives a good account of proton scattering from ^{12}C and ^{40}Ca. Other often-used interactions have Yukawa or Gaussian radial shapes with strengths and ranges chosen to reproduce low energy nucleon-nucleon scattering data. Comparisons between these various interactions are given in Ref. 25.

Many exchange mixtures other than the Serber mixture have been used in nuclear structure calculations. Often they have large odd-state components, thus differing from the forces predicted by realistic interactions. We have tried seven of the more commonly used structure forces[61] to see how their predictions for inelastic scattering compare with those for the central force which we use in this work. This force is an even state Yukawa force with a range of 1.4 F, and a strength chosen to be consistent with a recent survey of inelastic scattering analyses.[62] The results of this comparison will be presented in Sec. VIIC2.

For a zero-range force, it is clear from Eq. 9 that the form factor $G^{LSJ,T}_{(r_0)}$ is given by r^2 times the transition density. As the range of the two-body force increases, the form factor continues to reflect the radial shape of the transition density $F^{LSJ,T}_{(r_1)}$. This brings us back to the least well defined element in the cross section, namely, the transition density.

4. Transition Density

Referring back to Eqs. 6 and 7, we see that this quantity is determined by the wave functions which describe the states of the target nucleus. At this point it is useful to present a short review of the properties of single particle wave functions $u_{n\ell}$ which occur in the transition density. In this work we use harmonic oscillator wave functions, hence the single particle radial wave functions are completely specified by the principal quantum number n and the orbital angular momentum ℓ. The quantum number n specifies the number of nodes in the wave function; we use the convention that n starts from 1. We recall from Sec. IVA that the single particle orbitals which form the shell model basis are the $1g_{7/2}$, $2d_{5/2}$, $2d_{3/2}$, and $3s_{1/2}$. The single particle wave functions of interest in this work are therefore u_{14}, u_{22}, and u_{30}, which have 1, 2, and 3 nodes respectively. The transition density will be constructed from a sum of products of single particle wave functions, each product being weighted by the appropriate $M^{T}_{LSJ}(j_p j_h)$, which in turn is dependent upon the spectroscopic amplitude $Z^{JT}(j_h j_p)$. It is clear that a term such as $u_{14}u_{14}$ will contribute a simple shape with a single maximum, while a term such as $u_{22}u_{30}$ has several maxima and minima. An example of a typical transition density is that for the transition to the 2^+_1 state in ^{138}Ba. It is given by

$$F^{202,0}_{(r_1)} = -0.339u_{14}u_{14} + 0.135u_{14}u_{22} - 0.089u_{22}u_{22} + 0.031u_{22}u_{30}.$$

The coefficients $M^0_{202}(j_p j_h)$ are determined by the wave functions for the $0^+_{g.s.}$ and 2^+_1 states. Different wave functions will give different coefficients, and thus a transition density of different shape. This will in turn modify the shape of the form factor, and also the cross section, as discussed earlier. The magnitude of each $M^T_{LSJ}(j_p j_h)$ is related to the coherence properties of the amplitudes of the components of the wave functions; in general a larger $M^T_{LSJ}(j_p j_h)$ results from constructive interference between the amplitudes while a small number results from destructive interference. However, in our case the small size of the $M^T_{LSJ}(j_p j_h)$ involving the $2d_{3/2}$ or $3s_{1/2}$ orbitals is also in part due to the restriction on the occupation of these levels, as discussed in Sec. IVA. Hence, there are two aspects of the transition density which affect the cross section; the first being the magnitude of the individual components, and the second being the interference among the terms of the sum. Specific examples of transition densities will be illustrated in Sec. VIIC1, where we compare the transition densities for ^{138}Ba calculated with both the A=136-140 and A=136-145 sets of wave functions. We will find that one can easily distinguish the two sets of wave functions by virtue of the resulting transition densities and the angular distributions which they predict.

We note at this point that other methods exist for extracting the necessary transition density. One promising approach is through inelastic electron scattering.[63] It can be shown that the transition density is simply related to the measured

form factor in (e,e'), and high quality (e,e') data over a wide range of momentum transfer can fully determine the proton transition density, since electrons are mainly sensitive to protons in a nucleus. This can then lead to a determination of the neutron transition density if proper account is taken of core polarization effects.

Since 30 MeV protons are not strongly absorbed the cross section is sensitive not only to the tail of the transition density and its value in the vicinity of the nuclear surface as in (α,α'), but also to the transition density inside of the nucleus. For this reason, medium energy inelastic proton scattering provides a very sensitive test of the wave functions involved in a transition.

The previous discussion has been concerned only with the direct DWBA contribution to the scattering amplitude. The transition density is not defined as such for the exchange amplitude, since for exchange, the initial and final bound state wave functions have different radial co-ordinates. However, a quantity corresponding to $M^{T}_{LSJ}(j_p j_h)$ for the direct term exists for the exchange term,[25] and can be used to obtain an estimate of the magnitude of the exchange contribution to a given transition. In the case of the exchange amplitude, the form factor is different for each pair of partial waves, and involves many multipoles of the two-body force for an orbital angular momentum transfer L.

However, it has been found by a number of authors[25,64-66] that the direct and exchange amplitudes are constructively coherent in general, and identically so for a zero-range even state force. Atkinson and Madsen[29] have done a particularly complete study of the properties of the direct and exchange amplitudes for transitions in single closed shell nuclei (such as the N=82 nuclei). They find that with a Serber force the shapes of the exchange contributions to the angular distributions are very similar to those for the direct term. Since we have also used a Serber force, the previous transition density discussion appears to remain valid when the exchange amplitude is included in the cross section; the main effect of the exchange amplitude being a renormalization of the magnitude of the cross section.

5. Discussion of Selection Rules and Non-Normal Parity States

In terms of the transferred orbital angular momentum L, spin S, total angular momentum J, and isospin T, the selection rules for the direct amplitude in the DWBA are

$$\vec{J} = \vec{J}_f - \vec{J}_i$$

$$\vec{L} = \vec{J} - \vec{S} \qquad S = 0,1$$

$$\vec{T} = \vec{T}_f - \vec{T}_i \qquad T = 0,1$$

$$\Delta\pi = (-)^L$$

where $\Delta\pi$ denotes the change in parity. Both ^{138}Ba and ^{144}Sm have $J_i^\pi = 0^+$, so $J = J_f$.

For the exchange term in the DWBA amplitude, the selection rule $\Delta\pi=(-)^L$ no longer holds. Thus for exchange, all four triads (LSJ)-(J0J), (J1J), (J-1 1J), and (J+1 1J) can contribute to the cross section, while for the direct term, only the first or second pair can contribute depending on the parity change. The terms which the second pair of triads give rise to are commonly referred to as non-normal parity amplitudes and are found in general to be small except in the case of transitions to high spin states, where they can be important.[25]

The only experimental angular distributions for non-normal parity transitions (transitions to non-normal parity states for which $\pi\neq(-)^J$) in masses A>80 of which we are aware are those for the 3^+ and (5^+) states in ^{138}Ba, which we observe, and an angular distribution for a 4^- state in ^{208}Pb.[67] In all cases, the cross sections are less than 20 μb/sr at all angles. The fact that so few non-normal parity states are observed in inelastic proton scattering is evidence in itself that cross sections to such states must be small. Calculations for transitions to the 3^+ and (5^+) states in ^{138}Ba have been carried out and are described in detail in Sec. VIIC2. The resulting cross sections are approximately 1 μb/sr. Thus, both theory and experiment indicate that non-normal parity states (also often referred to as spin-flip states) are very weakly excited in medium energy inelastic proton scattering on heavy nuclei.

As mentioned in Sec. IVB, the pseudo spin-orbit coupling scheme of Hecht and Adler[47] predicts a selection rule for inelastic scattering. This selection rule is based on the assumption

that the transition densities are independent of the quantum numbers $j_p j_h$ and depend only on the orbital angular momentum transfer L. For (α,α') this is a reasonable assumption, since the alpha particles are strongly absorbed by the nucleus and are sensitive to the transition density only at the nuclear surface where, for the case of N=82 nuclei, the transition densities are quite similar as illustrated in Ref. 15. However, this may not be a good assumption for protons, which are not strongly absorbed. The selection rule states that $\Delta B=0$ where B is the total pseudo spin. For an even number of protons, B ranges from v/2 to 0, where v is the seniority of the state. The wave functions for ^{138}Ba which we have used have mixed seniority, but projecting out wave functions of good seniority reveals that the low-lying $J\neq 0$ states are more than 80% seniority two states. In the Hecht-Adler scheme, the lowest 2^+, 4^+, and 6^+ states have v=2, B=0 and transitions to these states from the v=0, B=0 ground state are allowed. Our data show them to be relatively strongly excited. The next group of states have v=2, B=1 so transitions to these states would violate the $\Delta B=0$ rule. With two exceptions, Fig. 2 shows that the positive parity states between 2.2-3.2 MeV are weakly excited. The third group of states predicted in the pseudo spin scheme are v=4, B=0 states. The relatively strong 2^+ states at 3339 and 3368 keV in ^{138}Ba are perhaps members of this group, since the shell model also predicts these levels to be mostly seniority four states.

We thus find that the pseudo spin orbit selection rules predict results which are in qualitative agreement with our data.

VII. DISCUSSION OF RESULTS

In this section we present results of the calculations described in Secs. IV and VI, and compare the theoretical predictions from those sections with the experimental results from Sec. III.

A. Comparison of Shell-Model Calculations to Experiment

We begin by contrasting the results of the shell model calculations for ^{138}Ba and ^{144}Sm described in Sec. IVA with the experimental energy level spectra obtained in Sec. IIIA. The energy level spectra for ^{138}Ba resulting from shell model calculations with both the A=136-145 and A=136-140 Hamiltonians, together with the experimental level spectrum as determined from our measurements, are shown in Fig. 14. The calculated energy level spectrum, using the A=136-140 interaction, is in excellent agreement with experiment. One-to-one correspondence between theory and experiment can be inferred up to 2.9 MeV of excitation, with the exception of the experimentally missing excited 0^+ state. Each of the states predicted by theory up to 2.85 MeV are in agreement with their experimental counterparts to within 200 keV, and for most states the agreement is better than 100 keV. In Sec. IIIC4 we noted that the angular distribution for the state

at 2201 keV did not enable us to assign this state $J^{\pi}=6^{+}$, although a 6^{+} assignment is not inconsistent with the data, as seen in Fig. 11. Comparing experiment to theory, one clearly finds additional support for a 6^{+} assignment to this state. The states at 2415 and 2445 keV, which have been assigned (5^{+}) and 3^{+} respectively,[40] have structureless angular distributions and are excited very weakly in our (p,p') measurements, thus leading us to concur with the non-normal parity assignments. These J^{π} assignments are also in excellent agreement with the shell model predictions. Recalling from Sec. IIIC3 the discussion of a 1^{+}-4^{+} doublet at 2583-2584 keV, we see such a proposal is strongly supported by predictions of the shell model.

In the discussion of Sec. IVA, we indicated that the parameters in the A=136-145 interaction may reflect deficiencies in the basis space for the upper N=82 isotones, since states of these isotones used in the determination of the interaction parameters may have configurations lying outside the present basis space. We observe from Fig. 14 that the A=136-145 interaction does not reproduce the ^{138}Ba energy levels with the accuracy of the A=136-140 Hamiltonian. The major differences are in the first 4^{+}-6^{+} splitting, and in the spacing of the levels from 2.3 to 2.6 MeV. A more sensitive test of the relative quality of the wave functions resulting from these interactions is found in the microscopic DWBA calculations, which will be discussed shortly.

The experimental energy level spectrum for ^{144}Sm along with the predicted energy level spectrum calculated from the A=136-145

interaction is shown in Fig. 15. The general characteristics of the experimental spectrum are reproduced; however the specific state-by-state agreement is not as impressive as the agreement between theory and experiment for ^{138}Ba. Allowing more than one proton to be excited into the $3s_{1/2}$ and $2d_{3/2}$ orbits, and including pairs of particles in the $1h_{11/2}$ orbit would be expected to improve the agreement between theory and experiment.

B. Collective Model Results

In this section we present the results of a collective model anlaysis of all states in ^{138}Ba and ^{144}Sm for which J^{π} assignments have been made. Figures 16 and 17 show our measured angular distributions for the lowest-lying 2^+, 3^-, 4^+, and 6^+ states in ^{138}Ba and ^{144}Sm, along with the collective model predictions for these states. The optical model parameters labeled Set SII (Set SI) in Table III had the lowest value of chi-square per point and were used in the calculations for ^{138}Ba(^{144}Sm), but any of the three sets give fits of similar quality. As seen in Figs. 16 and 17, the predicted angular distributions are in good agreement with the data for the 2^+ and 3^- states, but the agreement deteriorates as one goes to the higher spin states. Results of calculations for the remaining states observed in our measurements are not shown, since our use of characteristic shapes indicates that all experimental angular distributions for a given J^{π} are very similar in shape. The empirical observation that the shapes of the angular distributions appear to be independent of excitation energy in the

energy range from 1-3.5 MeV has been verified through the collective model DWBA calculations.

Deformation parameters β_L', as discussed in Sec. VIA, have been extracted by normalizing the experimental and theoretical cross sections over the angular range of the data. The results of this analysis are given in Table IV. The small size of these parameters, except for the lowest 3^- states, is another indication that the states are not strongly collective. Coulomb excitation was not included in the form factor calculations. Test cases showed that its inclusion would not have altered the extracted deformation parameters by more than four percent for $J^\pi=2^+$ and 3^-, and negligibly for higher spin transfers. Barker and Hiebert[18] have also studied ^{144}Sm(p,p') at 30 MeV, and the results of their collective model analysis are in good agreement with ours for the four states which they observe (see Table V). In addition, Woolam et al.[19] have measured β_2' for the inelastic scattering of 50 MeV protons (53 MeV ^{3}He) on ^{144}Sm, and find a value of $\beta_2'R'=0.41$ F ($\beta_2'R'=0.47$ F). Thus inelastic scattering of protons, ^{3}He, and alpha particles[18] leaving ^{144}Sm in it's first excited state yield values of $\beta_2'R'$ ranging from 0.41 to 0.47. These values are all within the probable errors of the technique. Table V gives a summary of the measured deformation parameters for excited states of ^{138}Ba and ^{144}Sm.

In Table V we also list the isoscalar transition strengths G_L, in single particle units, calculated from Eqs. 2 and 3. Coulomb excitation measurements on ^{138}Ba[39] and ^{144}Sm[42] yield

B(E2) values of 442 ± 18 e^2F^4 and 500 ± 80 e^2F^4 respectively for transitions from the first excited states in these nuclei. These values correspond to 10.0 ± 0.4 and 11.0 ± 1.8 single particle units respectively. Comparing them with the corresponding values for G(L) from Table V indicates that the values of G(L) obtained from inelastic scattering are only 60%-80% of those obtained through Coulomb excitation, although in the case of ^{144}Sm the results are probably consistent within the errors of the determinations. This phenomenon persists for other nuclei in this mass region,[17] which seems to be the only region which does not exhibit equality between the isoscalar and electromagnetic transition rates when they are extracted using this model.

As one adds protons outside a closed core, one expects that the strength of collective excitations out of the core will increase and that this increase will be reflected in the inelastic-scattering cross sections. Barker and Hiebert[17,18] have noted such an increase in strength for the lowest lying 3^- state but have found no increase for the lowest lying 2^+ state. To check on this expectation with our more complete data, we have summed the strengths found for the 2^+, 3^-, and 4^+ states in Figs. 6-10, with the results shown in Table VI. The strengths of the 2^+ excitations differ by 35% while the 3^- and 4^+ excitations are about a factor of two stronger in ^{144}Sm. The only unassigned states ($E_x \lesssim 3.3$ MeV) with substantial strength are in ^{144}Sm and these probably have $L \geq 4$, which would tend to increase the ratio for the higher spins. The sample of 6^+ states is so small, no reliable conclusions can be drawn, but the ratio is less than 1 if the cross sections in Fig. 11 are assigned to be 6^+.

It has been suggested[51] that a better measure of the strength is the energy weighted sum $\Sigma E_x G_L$. The ratios of these sums are also tabulated in Table VI. The ratio for the 2^+ states is essentially unchanged, while that for the 3^- states is now near unity and that for the 4^+ states is somewhat increased.

C. Microscopic Model Analysis

As discussed in the introduction, one of the main purposes in undertaking this work was to determine whether large basis shell-model wave functions could accurately account for both the shape and magnitude of measured angular distributions obtained from inelastic proton scattering. To this end, we have applied the microscopic DWBA theory discussed in Sec. VIB to calculate angular distributions for the 2_1^+, 2_2^+, 4_1^+, 4_2^+, and 6_1^+, 6_2^+ states observed in ^{138}Ba and ^{144}Sm.

The pertinent details of the inelastic scattering calculation are as follows. The optical model parameters labeled Set SII (Set SI) in Table III are used to describe the incident and exit channels of ^{138}Ba(^{144}Sm). The bound states are described by harmonic oscillator wave functions, with an harmonic oscillator constant obtained from Eq. 8. The two-body interaction between the projectile and target nucleons was central only, with the Serber exchange mixture and a Yukawa radial dependence. Thus we have

$$V_{ip}(r) = [V_{00} + V_{10}\vec{\sigma}_i\cdot\vec{\sigma}_p + V_{01}\vec{\tau}_i\cdot\vec{\tau}_p + V_{11}(\vec{\sigma}_i\cdot\vec{\sigma}_p)(\vec{\tau}_i\cdot\vec{\tau}_p)]\frac{e^{-r/\alpha}}{r/\alpha}$$

where α is the range of the force, i, p label the valence nucleons and the projectile, respectively and the subscripts on the V_{ST} are the spin and isospin transferred in the reaction. For a Serber interaction $V_{00}:V_{10}:V_{01}:V_{11} = -3:1:1:1$. The strength of the largest of the V_{ST} was taken as the mean value found in the tabulation of Austin,[62] $V_{00}=-27.8$ MeV for a range $\alpha=1.0$ F. It was found in preliminary calculations that $\alpha=1.4$ F provided a somewhat better fit to the shape of the angular distributions. The value of $V_{00}(\alpha=1.4\ F)=-12.6$ MeV used in the calculations was fixed so as to give the same cross section in a DWBA calculation for the 2_1^+ state in ^{138}Ba as did the 1.0 F range force. Since our wave functions contain only proton orbitals, the number which actually enters the calculations is $V_{pp}^S=V_{S0}+V_{S1}$, which is -8.4 MeV for the dominant S=0 part of the proton-proton interaction. Coulomb excitation was not included in the calculations.

Core polarization, i.e., the effect due to contributions to the cross section from nucleons outside the explicit shell-model basis space, must be included for a proper description of inelastic scattering.[68] In the case of electromagnetic transitions these effects also appear and are accounted for by renormalizing the charge on the nucleons, i.e., by introducing a "polarization charge". Madsen[29,30] has shown that one can similarly correct for finite basis-space effects in inelastic scattering by renormalizing the strength of the two-body force which mediates the transition. Thus one has an "effective force" for (p,p') which is analogous to the "effective charge" for electromagnetic transitions.[69]

Madsen's result[29] for the renormalization factor ε is

$$\varepsilon = \frac{V_{00}e_0(L)+V_{01}e_1(L)}{V_{00}+V_{01}} \qquad \text{(Eq. 10)}$$

where e_0 and e_1 are defined in terms of the total effective charges on the neutron and proton; $e_0=e_p+e_n$, $e_1=e_p-e_n$. The major assumption involved in obtaining this result is that the ratios of the inelastic scattering single particle amplitudes (direct plus exchange) to the corresponding electromagnetic amplitudes are independent of the single particle quantum numbers. This is rigorously true for the direct amplitude in the plane wave Born approximation at zero momentum transfer. Madsen[29] has shown by numerical calculation for ^{118}Sn that it is true within a 9% effect on ε for a DWBA calculation including the exchange amplitude.

One can estimate the enhancement factor directly from Madsen's formula. However, we prefer to proceed in a more heuristic fashion to make the input assumptions clear. To get an idea of the core participation in the low-lying states of ^{138}Ba, we note that for the wave functions used here, the calculated B(E2; $2_1^+ \rightarrow 0_1^+$) is a factor of 3.2 too small[69] if no polarization charge δe is used. This implies that $(1+\delta e)^2=3.2$, or $\delta e=0.8$. To account for the contribution to the (p,p') reaction of protons excited from the core, one therefore renormalizes the interaction strength V_{pp} to $(1+\delta e)V_{pp}$. However, neutron core excitations also contribute to (p,p') cross sections and are, in fact, more important than those for protons, since the proton-neutron two-body interaction V_{pn} is stronger than V_{pp}. If it is assumed, as has been found by

Bernstein[70] and Astner, et al.[71] that contributions from neutron and proton core excitations are approximately in the ratio of N/Z (the ratio expected in a collective model picture), we need an additional term, N/Z δ_e V_{pn}. For the Serber exchange mixture we use, $V_{pn}=2V_{pp}$. Thus one obtains a total effective force of $(1+\delta_e)V_{pp}+2N/Z\delta_e V_{pp}=[1+\delta_e(1+2N/Z)]V_{pp}$, i.e. the strength is increased by a factor of $(1+\delta_e(1+2N/Z))$. This corresponds to a cross section enhancement of 17.2. We have also inverted this process and used the measured enhancement factors to extract polarization charges for other transitions in ^{138}Ba, for which electromagnetic transition data are not available. Calculations of cross sections were performed for the 2_1^+, 2_2^+, 4_1^+, 4_2^+, 6_1^+, and 6_2^+ states in ^{138}Ba. The enhancement factors were extracted by normalizing the experimental and theoretical integrated cross sections over the angular range of the data.

To estimate the accuracy of the polarization charges, we consider the effects of uncertainties in the input numbers. First of all, V_{00} is perhaps known to within $\pm$15%, which corresponds to an uncertainty of $\pm$0.16 in δ_e. Uncertainties introduced by possible variations from a Serber force are not large (<0.04 in δ_e) because, for example, an increase in V_{01} leads to a decrease in $|V_{pp}|$ but an increase in V_{pn}/V_{pp}, and these effects almost cancel. If we assign to the ratio of neutron and proton polarization changes a fifty percent uncertainty, $\delta n/\delta p=N/Z=1.46\pm0.23$, the corresponding uncertainty in δ_e is $\pm$0.10. The usual DWBA

uncertainties for inelastic scattering are perhaps $\pm$20% in cross section corresponding to an uncertainty in δe of $\pm$0.11. Finally the uncertainty of $\pm$10% in the experimental normalization contributes an uncertainty of $\pm$0.05. Adding these in quadrature one obtains an uncertainty of $\Delta(\delta e)=0.23$. Most of these effects change the numbers for different L transfers in the same way so the relative values of δe_p are perhaps better known than this. On the other hand, we have neglected the basic uncertainty in the approximation of Eq. 10. If Madsen's estimate for ^{118}Sn (2^+) were valid here, our numbers would be large by 0.1. It is possible the overestimate is larger for the higher spin states where exchange effects are more important but we have no direct evidence for this. The results of our analysis of δe are shown in Table VII, and we see that the δe are constant within the probable overall uncertainty in the analysis.

1. Microscopic DWBA Calculations for ^{138}Ba

For ^{138}Ba, we have calculated angular distributions using both sets (A=136-140 and A=136-145 Hamiltonians) of wave functions for the aforementioned 6 states. Figures 18 and 19 show the angular distributions predicted by each set of wave functions, together with the appropriate data. All theoretical cross sections include an enhancement factor calculated with $\delta e=0.8$, i.e., they have not been individually normalized to the data but represent an essentially a priori calculation. The knock-on exchange amplitude contributes substantially to all cross sections and especially to those for the

high spin states. We see that the magnitudes and shapes of the calculated angular distributions are in good agreement with the data for the 2_1^+, 4_1^+, and 6_1^+ states for both sets of wave functions. However, the agreement between theory and experiment for the 2_2^+, 4_2^+, and 6_2^+ states is much better for the A=136-140 set of wave functions than for the A=136-145 set, which predicts cross sections which are an order of magnitude low, and also exhibit poorer agreement in shape. From this analysis it appears that the A=136-140 set of wave functions gives the better description of the low-lying states of ^{138}Ba.

To find the reason for this behavior, recall from Sec. VIB4 that all of the nuclear structure information entering the DWBA calculation is contained in the transition densities. Thus it is informative to compare the differences in their structure as calculated from each set of wave functions. Figure 20 shows such a comparison. The magnitude of the transition density is plotted versus the radial coordinate expressed in units of $r_o A^{1/3}$; thus unity corresponds to the nuclear surface. Inspection shows that the transition densities for the 2_1^+, 4_1^+, and 6_1^+ states are quite similar for both sets of wave functions. They peak slightly inside the nuclear surface, which is a general characteristic[55] of these quantities. We recall that the cross sections calculated for these states were very similar for both sets of wave functions. However, there are distinct differences in the transition densities for the 2_2^+, 4_2^+, and 6_2^+ transitions. The A=136-145 wave functions yield

transition densities with a pronounced decrease of the surface peaking, and an increase in magnitude of the peak near 0.6 of the nuclear radius, relative to the A=136-140 results. For the 6_2^+ state, this effect is so great that the transition density resembles that for a much lighter nucleus. Since the transition density (and therefore the form factor) peaks too far inside the nuclear surface for this transition, the diffraction pattern predicted by the DWBA is pushed out, as if the target nucleus were indeed much lighter. This is exactly what we observe for the calculated 6_2^+ cross section for the A=136-145 set of wave functions.

We can infer specifically what is wrong with this set of wave functions by considering the individual contributions to the total transition density for the 6_2^+ state, for example. Figure 21 shows both this transition density and its component parts proportional to $u_{14}u_{14}$ and $u_{14}u_{22}$. For the A=136-140 set of wave functions the $u_{14}u_{22}$ term is large relative to the $u_{14}u_{14}$ term, which results in the surface peaking. However, the components are about the same size for the A=136-145 wave functions, and the transition density is very small at the surface due to a cancellation effect. Tracing back one step farther, we can look at the spectroscopic amplitudes which contribute to $u_{14}u_{14}$ and $u_{14}u_{22}$ and thus directly study the wave functions. Only the $M^T_{LSJ}(j_p j_h)=M^0_{606}(g_{7/2},g_{7/2})$ matrix element contributes to $u_{14}u_{14}$, while both $M^0_{606}(g_{7/2}d_{5/2})$ and $M^0_{606}(d_{5/2},g_{7/2})$ contribute to the

$u_{14}u_{22}$ term of the sum. Table VIII shows the structure of the largest components of the pertinent wave functions, as well as the individual contributions to the 6_2^+ transition density calculated with both sets of wave functions. The two transition densities are thus

$$F^{606,0}_{(r_1)} = 0.1292\ u_{14}u_{14} + 0.3223\ u_{14}u_{22} \qquad \text{A=136-140}$$

$$F^{606,0}_{(r_1)} = 0.1765\ u_{14}u_{14} + 0.1978\ u_{14}u_{22} \qquad \text{A=136-145}$$

The quantity of interest is the ratio $u_{14}u_{22}/u_{14}u_{14}$ which has the value 2.50(1.12) for the A=136-140 (A=136-145) interaction. The major reason for the smaller ratio from the A=136-145 wave functions is the small size of the $u_{14}u_{22}$ contribution. This set of wave functions has the smaller $g_{7/2}$-$d_{5/2}$ single particle splitting and might naively be expected to have the larger $u_{14}u_{22}$ term; a detailed comparison of the wave functions in Table VIII shows why this is not so. The largest contributions to $u_{14}u_{22}$ for the A=136-140 set come from the $(g_7)^6 \rightarrow (g_7)^5(d_5)^1$ and $(g_7)^4(d_5)^2 \rightarrow (g_7)^4(d_5)^2$ amplitudes, which for the A=136-145 wave functions are much smaller. This is because the smaller $g_{7/2}$-$d_{5/2}$ splitting leads to a fragmentation of the strength of the 6_2^+ wave function over many components. Many of these components cannot be connected by the one body (p,p') operator to the strong components of the much less fragmented ground state, and hence do not contribute significantly to the transition density. It thus appears that this decreased mixing between the $g_{7/2}$ and $d_{5/2}$ orbitals is the required ingredient in obtaining a

reasonable fit to the angular distribution for the 6_2^+ state. A similar analysis applied to the transition densities for the 4_2^+ states arrives at the same conclusion--namely that there appears to be too much mixing of the $g_{7/2}$-$d_{5/2}$ orbitals in the higher lying states as calculated with the A=136-145 interaction. Specific information concerning the structure of the wave functions can thus be obtained by analyzing the composition of the transition densities in this manner.

Comparing the DWBA calculations resulting from the collective model (Fig. 16) and microscopic model (Fig. 18) for the 2_1^+ state, we see that the collective model does a somewhat better job of fitting the data. We have performed a collective model calculation using the form factor obtained by deforming only the real part of the optical model potential, and obtained an angular distribution nearly identical to the angular distribution obtained from the microscopic model. This implies that if one were to combine the form factor obtained by deforming the imaginary part of the optical model with the real form factor used in the microscopic analysis, the resulting angular distribution would be in as good agreement with the data as that of the full deformed collective model. Unfortunately, the computer code we use for the microscopic DWBA calculations does not at present have the option of using a complex form factor; thus the above conclusion is rather speculative. However, it has recently been found that using a complex microscopic form factor results in appreciably better fits to angular

distribution[72] and asymmetry[73] data. It would also be interesting to determine whether the addition of an imaginary term to the form factor, which appears to improve the fit to the 2_1^+, would destroy the relatively good fits to the 4_1^+ and 6_1^+ states obtained with the present microscopic approach.

It must be noted that our calculations use a multiplicative constant in the form factor to account for core polarization and the angular distributions have the shape predicted by the purely microscopic calculation. Other microscopic calculations[68] have frequently employed an additive term in the form factor based on the collective model to simulate the effects of core polarization. Often times, using this latter procedure, the collective term is the dominant contributor to the cross section, so the predicted shape for the angular distribution is in reality due to the collective model contribution. Thus, these "microscopic" calculations achieve good agreement with the data as regards the shape of the angular distribution, due to the fact that collective model predictions for the shape are in general better than those calculated from a purely microscopic model such as we have used.

The above considerations seem to argue for the use of an additive collective model form factor to account for core polarization effects. However, the effective charge approach has the important advantage of reflecting the apparent physical fact that the participation of the core is approximately proportional to the transition strength due to the valence orbitals alone. In the case of the 2^+ states in ^{138}Ba for example, the cross

section (and hence the core contribution) for the 2_1^+ state is about four times that for the 2_2^+ state. Yet both are given correctly by the same multiplicative renormalization.

2. Calculations with Other Forces

A Serber exchange mixture, which is an even-state force, is commonly employed in microscopic inelastic scattering calculations. However, in nuclear structure calculations, many other types of forces have been employed, and we have tried a number of these to see if they give as good a description of the inelastic scattering process as the Serber mixture. We have made calculations for each of the forces "Cal", "Cop", Clark Elliot I, Ferrell-Visscher, Rosenfeld and Soper (summarized in Ref. 61), all of which contain non-negligible odd-state components. The triplet-even parts of the various forces have all been normalized to V_{TE}=-40 MeV. In each case, the force had a Gaussian radial shape with a range of 1.67 F; this translates into 1.3 F for the Yukawa radial dependence which we use. The strength of the Serber force is very similar to the strength we have used in the calculations discussed previously. The results are shown in Table IX, along with the results obtained with the Serber mixture.

We observe that only the Clark-Elliot I and Soper interactions (which have weak odd state components) yield results similar to the Serber mixture which reproduced the data. For the forces with strong odd-state components the direct and exchange cross sections have the wrong dependence upon L-transfer and in addition, the theoretical angular distributions often

acquire shapes which do not resemble the data. We conclude that while such forces may be acceptable for nuclear structure calculations, the strong odd-state components probably make them inadequate to describe inelastic proton scattering.

We have performed calculations including tensor forces corresponding to the one-pion-exchange potential,[62] and find that the tensor force contributions to the cross section are at most 7%, and this is for the 6^+ states, where the non-normal exchange amplitudes are becoming non-negligible.[25] The spin-orbit force may be important[74] for the 6^+ states; this possibility is being investigated further.

Finally, we have calculated cross sections for transitions to the non-normal parity 3^+ and (5^+) states at 2.445 and 2.415 MeV, respectively. These cross sections are not expected to be strongly affected by collective effects, but may be sensitive to tensor and spin-orbit terms in the effective interaction. The tensor force used corresponded[62] to the one-pion-exchange potential while the spin-orbit force was obtained from the Hamada-Johnston potential with a cutoff radius of 0.6 F as described in Ref. 62; this force is somewhat weaker than that used by Love.[74] As is seen in Fig. 22, the tensor and spin-orbit forces are indeed important, but the theoretical cross section is a factor of 3-5 below the data. More complex reaction mechanisms such as those involving multistep processes may be important for these weakly excited states.

3. Microscopic DWBA Calculations for ^{144}Sm

Only the A=136-145 Hamiltonian was applicable to ^{144}Sm, so only the set of wave functions corresponding to this interaction was employed in the DWBA calculations. For comparison purposes we have used the same enhancement factor (17.2) as for ^{138}Ba. This corresponds to a polarization charge of 0.8, which is close to the value 1.02 ± 0.17 obtained from the measured B(E2) value[42] and the A=136-145 wave functions. The results are shown in Fig. 23. The D+E angular distribution for the 4_1^+ state is a factor of two smaller than the data at forward angles, but the inadequacy of the basis space for ^{144}Sm is most clearly pointed out when one considers the calculation for the 2_2^+ state. All of the strength has been concentrated in 2_1^+, causing the angular distribution for the 2_2^+ state to fall a factor of 25 below the data. In addition, the shape is not qualitatively correct; the maxima at 40° is larger than the first at 20°. The calculated 4_2^+ angular distribution is a factor of 3 lower than the data, while the calculation for the 6_2^+ bears no resemblance to the data. This can easily be predicted from observation of the transition density for the 6_2^+ state; it is negligible at the surface of the nucleus. All of its strength is concentrated around 0.6 of the nuclear radius, as in the similar case for the 6_2^+ transition density in ^{138}Ba calculated with the A=136-145 set of wave functions. As is obvious from Fig. 23 a constant polarization charge does not reproduce the magnitude of the angular distribution for

different L-transfers. One is required to use a state dependent polarization charge, whereas a state independent charge was found to be adequate for states in ^{138}Ba.[32] This presumably is also a manifestation of the limited basis space for the ^{144}Sm shell-model calculation.

VIII. SUMMARY

Cross sections for the inelastic scattering of protons from ^{138}Ba and ^{144}Sm were measured with a resolution of 7-10 keV at 30 MeV bombarding energy. We have obtained excitation energies for levels in ^{138}Ba which are in excellent agreement with previous gamma ray work on this nucleus, and in addition we have been able to reduce the uncertainty on previous spin-parity assignments, in most cases suggesting a precise assignment. We have increased the number of known levels up to E_x=3.4 in ^{144}Sm from 8 to 18 and made spin-parity assignments for the majority of these states. The experimental information concerning the levels up to E_x=3.4 MeV in ^{138}Ba and ^{144}Sm has been reviewed, and found to be in good agreement with recent shell-model calculations for this region. For ^{138}Ba there is essentially one-to-one agreement between experiment and shell-model calculations up to E_x=2.9 MeV, with observed and predicted states typically lying within 100 keV of each other.

Collective model DWBA calculations have been carried out for both nuclei, using a form factor obtained by deforming the real and imaginary parts of the optical model potential. The results were analyzed using the formalism of Bernstein to obtain estimates

of the strengths of the corresponding electromagnetic transition rates.

Microscopic DWBA calculations including the exchange amplitude were performed for the $2^+_{1,2}$, $4^+_{1,2}$, and $6^+_{1,2}$ states in ^{138}Ba and ^{144}Sm, using shell model wave functions,[27,28] a realistic two-nucleon force, and an enhancement factor calculated using the effective charge model of Madsen.[29,30] The necessary structure amplitudes were calculated with a modified version of the Oak Ridge-Rochester shell model code. In the case of ^{138}Ba, calculations were made with two sets of shell model wave functions and it was determined that inelastic proton scattering cross sections clearly distinguished one set as quite satisfactory and and superior to the other. The transition densities, which provide the link between the wave functions and the DWBA reaction model, were analyzed to see if one could determine the undesirable properties of the poorer set of wave functions. The results of this analysis indicated that the large mixing between the $g_{7/2}$ and $d_{5/2}$ orbitals was the problem in the set of wave functions which yielded the poorer result. We find that a careful consideration of the transition density between two states can provide useful information concerning the structure of the wave functions for these states. Predictions of the cross sections for ^{144}Sm were much less satisfactory than those for ^{138}Ba, presumably because the chosen shell model basis is rather restricted in the ^{144}Sm case.

The contributions to the cross section of core excitations were stronger by about a factor of 20 than those of the valence protons for the low-lying 2^+, 4^+, and 6^+ states of ^{138}Ba and ^{144}Sm. However, in the case of ^{138}Ba it was found that a state and multipole independent effective charge described the core polarization contributions to the cross sections within about 25%. This implies that the core participation for a given state in ^{138}Ba is approximately proportional to the transition strength due to the valence orbitals.

It is perhaps worth pointing out here that inelastic proton scattering is extremely sensitive to neutron configurations because the proton-neutron force is approximately twice the proton-proton force. This sensitivity is what leads to an enhancement factor of 17.2 in the (p,p') cross section, over five times larger than the corresponding enhancement of electromagnetic transitions (3.2). It also makes (p,p') studies a valuable complement to inelastic electron scattering, which is mostly sensitive to proton configurations, in studies of the isospin structure of core excitations.

Finally we note that the program developed in this work for the calculation of the spectroscopic amplitudes was a modification of the Oak Ridge-Rochester shell model codes[26] and can be used whenever wave functions obtained with this code are available. Such wave functions are now available for most nuclei up through the nickel isotopes, and for the zirconium, N=82, and lead regions, making possible for the first time to treat inelastic scattering

in a consistent microscopic fashion over a large part of the nuclidic chart.

ACKNOWLEDGEMENTS

We wish to thank H. McManus and F. Petrovich for enlightening conversations and assistance, and R. Schaeffer for making the code DWBA70 available. We are also grateful to J. McGrory for assistance with the Oak Ridge-Rochester shell model codes, and to S. Fox for his assistance in the data taking.

REFERENCES

1. B.H. Wildenthal, E. Newman, and R.L. Auble, Phys. Rev. C3, 1199(1971).
2. W.P. Jones, L.W. Borgman, K.T. Hecht, J. Bardwick, and W.C. Parkinson, Phys. Rev. C4, 580(1971).
3. R.K. Jolly and E. Kashy, Phys. Rev. C4, 887(1971).
4. R.K. Jolly and E. Kashy, Phys. Rev. C4, 1398(1971).
5. D. von Ehrenstein, G.C. Morrison, J.A. Nolen, and N. Williams, Phys. Rev. C1, 2066(1970).
6. P.A. Moore, P.J. Riley, C.M. Jones, M.D. Mancusi, and J.L. Foster, Jr., Phys. Rev. C1, 1100(1970); P.A. Moore, P.J. Riley, C.M. Jones, M.C. Mancusi, and J.L. Foster, Jr., Phys. Rev. Letters 22, 356(1969); G.C. Morrison, N. Williams, J.A. Nolen, Jr., and D. von Ehrenstein, Phys. Rev. Letters 19, 592(1967); P. von Brentano, W.J. Braithwaite, J.G. Cramer, W.W. Eidson, and G.W. Phillips, Phys. Letters 26B, 448(1968); K. Mudersbach, A. Heusler, and J.P. Wurm, Nucl. Phys. A146, 477(1970).
7. John C. Hill and D.F. Fuller, Phys. Rev. C5, 532(1972).
8. L.C. Carraz, E. Monnand, and A. Moussa, Nucl. Phys. A171, 209(1971).
9. M.A.J. Mariscotti, W. Gelletly, J.A. Moragues, and W.R. Kane, Phys. Rev. 174 , 1485(1968).
10. P. Van der Merwe, I.J. Van Heerden, W.R. McMurrray, and J.G. Malan, Nucl. Phys. A124, 433(1969).
11. J. Kownacki, H. Ryde, V.G. Sergejev, and Z. Sujkowski, Nucl. Phys. A196, 498(1972).

12. B. Arad, G. Ben-David, Y. Schlesinger, and M. Hass, Phys. Rev. C6, 670(1972).

13. O. Hansen and O. Nathan, Nucl. Phys. 42, 197(1963).

14. Per Rex Christensen and Fu-Chia-Yang, Nucl. Phys. 72, 657(1965).

15. F.T. Baker and R. Tickle, Phys. Rev. C5, 182(1972).

16. H.W. Baer, H.C. Griffin, and W.S. Gray, Phys. Rev. C3, 1398(1971).

17. J.H. Barker and J.C. Hiebert, Phys. Rev. C6, 1795(1972).

18. J.H. Barker and J.C. Hiebert, Phys. Rev. C4, 2256(1971).

19. P.B. Woollam, R.J. Griffiths, and N.M. Clarke, Nucl. Phys. A189, 321(1972); P.B. Woollam, et al., Nucl. Phys. A179, 659(1972).

20. R.H. Bassel, G.R. Satchler, R.M. Drisko, and E. Rost, Phys. Rev. 128, 2693(1962).

21. H.G. Blosser, G.M. Crawley, R. deForest, E. Kashy, and B.H. Wildenthal, Nucl. Instr. and Methods 91, 1(1971).

22. S.M. Austin, P.J. Locard, S.N. Bunker, J.M. Cameron, J.R. Richardson, J.W. Verba, and W.T.H. vanOers, Phys. Rev. C3, 1514(1971).

23. R. Reif and J. Höhn, Nucl. Phys. A137, 65(1969).

24. G.R. Satchler, Nucl. Phys. 77, 481(1966).

25. W.G. Love and G.R. Satchler, Nucl. Phys. A159, 1(1970).

26. J.B. French, E.C. Halbert, J.B. McGrory, and S.S.M. Wong, in Advances in Nuclear Physics, Vol. III, eds. M. Baranger and E. Vogt (Plenum Press, New York, 1969).

27. B.H. Wildenthal, Phys. Rev. Letters 22, 1118(1969).

28. B.H. Wildenthal and D. Larson, Phys. Letters 37B, 266(1971).

29. J. Atkinson and V.A. Madsen, Phys. Rev. C1, 1377(1970).

30. H. McManus, in The Two-Body Force in Nuclei, eds. S.M. Austin and G.M. Crawley (Plenum Press, New York, 1972).

31. D. Larson, S.M. Austin, and B.H. Wildenthal, Phys. Letters 41B, 145(1972).

32. D. Larson, S.M. Austin, and B.H. Wildenthal, Phys. Letters 42B, 153(1972).

33. R.K. Jolly, G.F. Trentelman, and E. Kashy, Nucl. Instr. and Methods 87, 325(1970).

34. D.L. Bayer, Ph.D. Thesis, Michigan State University 1970 (unpublished).

35. B.L. Cohen, Rev. Sci. Instr. 30, 415(1959).

36. G.F. Trentelman and R.G.H. Robertson, unpublished.

37. F.D. Becchetti, Jr., and G.W. Greenlees, Phys. Rev. 182, 1190(1969).

38. G.R. Satchler, Nucl. Phys. A92, 273(1967).

39. J.R. Kerns and J.X. Saladin, Phys. Rev. C6, 1016(1972).

40. E. Achterberg, F.C. Iglesias, A.E. Jech, J.A. Moragues, D. Otero, M.L. Perez, A.N. Proto, J.J. Rossi, W. Scheuer, and J. F. Suarez, Phys. Rev. C5, 1759(1972).

41. J. Kownacki and K.G. Rensfelt, Phys. Letters 35B, 153(1971).

42. D. Eccleshall, M.J.L. Yates, and J.J. Simpson, Nucl. Phys. 78, 481(1966).

43. S. Raman, Private Communication.

44. M. Rho, Nucl. Phys. 65, 497(1965).

45. M. Waroquier and K. Heyde, Nucl. Phys. A164, 113(1971).

46. V. Gillet and M. Rho, Phys. Letters 21, 82(1966).

47. K.T. Hecht and A. Adler, Nucl. Phys. A137, 129(1969).

48. G.W. Greenlees and G.J. Pyle, Phys. Rev. 149, 836(1966).

49. S.A. Fulling and G.R. Satchler, Nucl. Phys. A111, 81(1968).

50. D.L. Show, unpublished.

51. A.M. Bernstein, in Advances in Nuclear Physics, Vol. III, eds. M. Baranger and E. Vogt (Plenum Press, New York, 1969).

52. R. Schaeffer and J. Raynal, unpublished.

53. J. Raynal, Nucl. Phys. A97, 572(1967).

54. V.A. Madsen, Nucl. Phys. 80, 177(1966).

55. F. Petrovich, Michigan State University Thesis, 1970 (unpublished).

56. J. Blomqvist and A. Molinari, Nucl. Phys. A106, 545(1968).

57. T. Hamada and I.D. Johnston, Nucl. Phys. 34, 382(1962).

58. S.A. Moszkowski and B.L. Scott, Annals of Phys. 11, 65(1960).

59. F. Petrovich, H. McManus, V.A. Madsen, and J. Atkinson, Phys. Rev. Letters 22, 895(1969).

60. A. Kallio and K. Kolltveit, Nucl. Phys. 53, 87(1964).

61. V. Gillet, A.M. Green, and E.A. Sanderson, Nucl. Phys. 88, 321(1966).

62. S.M. Austin in The Two-Body Force in Nuclei, eds. S.M. Austin and G.M. Crawley (Plenum Press, New York, 1972).

63. R.M. Haybron, M.B. Johnson, and R.J. Metzger, Phys. Rev. 156, 1136(1967).

64. J. Atkinson and V.A. Madsen, Phys. Rev. Letters 21, 295(1968).

65. K.A. Amos, V.A. Madsen, I.E. McCarthy, Nucl. Phys. A94, 103(1967).

66. H.V. Geramb and K.A. Amos, Nucl. Phys. A163, 337(1971).

67. A. Scott, private communication.

68. W.G. Love and G.R. Satchler, Nucl. Phys. A101, 424(1967).

69. D. Larson and B.H. Wildenthal, B.A.P.S. 17, 512(1972).

70. A.M. Bernstein, Phys. Letters 29B, 335(1969).

71. G. Astner, I. Bergström, J. Blomqvist, B. Fant, and K. Wikström, Nucl. Phys. A182, 219(1972).

72. G.R. Satchler, Phys. Letters 35B, 279(1971).

73. R.H. Howell and G.R. Hammerstein, Nucl. Phys. A192, 651(1972).

74. W.G. Love, Phys. Letters 35B, 371(1971).

75. E.C. Halbert, J.B. McGrory, B.H. Wildenthal, and S.P. Pandya, in Advances in Nuclear Physics, Vol. IV, eds. M. Baranger and E. Vogt (Plenum Press, New York, 1972).

Table I: Energy levels of ^{138}Ba and ^{144}Sm.

^{138}Ba				^{144}Sm			
Present Work $E_x[J^\pi]^{a,d}$			Previous Work $E_x[J^\pi]^b$	Present Work $E_x[J^\pi]^{a,d}$			Previous Work $E_x[J^\pi]^c$
1436[g]	±1.0	2^+	1435.7±0.2 2^+	1661[g*]	±1.0	2^+	1660.6±1.0 2^+
1898[g*]	±1.0	4^+	1898.4±0.3 4^+	1811[g]	±1.2	3^-	1810.1±0.5 3^-
2090[g*]	±1.0	6^+	2090.1±0.6 (6^+)	2191[g*]	±1.0	4^+	2190.6±1.0 4^+
2201	±2.0		2203.2[f]	2324[e]	±1.0		2323.2±0.5 6^+
2218	±1.0	2^+	2217.9±0.4 2	2423*	±1.0	2^+	2423.4±1.0
2308*	±1.0	4^+	2307.4±0.3 (3,4)	2478	±1.9		2478.3±1.0 0^+
2415	±1.2		2414.9±0.6 (5^+)[h]	2588	±1.0	4^+	
2445	±1.2		2445.4±0.3 3^+[h]	2661	±1.6		
			2582.8±0.6 1,2	2800	±1.6	2^+	
2584	±1.0	4^+		2826	±1.8		2830 ±10
2639	±1.2	2^+	2639.3±0.4 2	2883	±1.9	4^+	
2779*	±1.0	4^+	2779.2±0.5 2,3,4	3020	±2.0	4^+	
2881[g]	±1.2	3^-	2880.5±0.6 3^-	3080	±2.0		
(2929)[i]	±2.0		2931.1±1.0 1,2	3123	±1.8		3123.8±1.0 $7^{(-)}$
(2990)[i]	±2.0		2990.8±0.5 1,2,3,4	3196	±1.9		
3050*	±1.0		3049.9±1.0 1,2	3227	±2.0	3^-	
3156	±1.2	4^+		3266	±2.3		
			3163.5±0.8 2,3,4	3308	±2.1	6^+	
3254	±1.2						
3285	±1.4						
3339	±1.4	2^+	3339.5±1.5 1,2				
			3352.2±1.5 1,2				
3368	±1.8	2^+	3365.9±1.0 1,2				

[a] Excitation energies in keV.

[b] From Ref. 7, except see (f,h) below.

[c] From Ref. 11,18 and references cited therein and Ref. 43.

[d] Subset of levels used in energy calibration is marked with an asterisk(*)

[e] Unresolved doublet whose angular distribution is consistent with a spin 6^+ state plus a lower spin state.

[f] From Ref. 8.

[g] Used in determination of characteristic shapes.

[h] From Ref. 40.

[i] These states were observed only at 200

Table II. Parameters of the MSDI $V=-4\pi A\delta(r_i-r_j)f_{ij}+B$[a] and single particle energies used for the calculation of the wave functions.

Parameter	A=136-140 Interaction [MeV]	A=136-145 Interaction [MeV]
A	0.373	0.382
B	0.507	0.517
$E_{g_{7/2}}$	-9.526	-9.451
$E_{d_{5/2}}$	-8.646	-8.970
$E_{d_{3/2}}$	-6.626	-6.334
$E_{s_{1/2}}$	-6.576	-6.438
$E_{g_{7/2}}-E_{d_{5/2}}$	0.880	0.481
$E_{g_{7/2}}-E_{d_{3/2}}$	2.900	3.117
$E_{g_{7/2}}-E_{s_{1/2}}$	2.950	3.013

[a]The notation is that used in Ref. 75.

Table III. Optical model parameters for $^{138}Ba(^{144}Sm)$. Potential strengths are in MeV, distances in F, and cross sections in mb.

	Adjusted Becchetti-Greenlees		Satchler Set SI		Satchler Set SII	
r_c	1.25	(1.25)	1.2	(1.2)	1.2	(1.2)
V_R	53.26	(53.20)	56.80	(56.10)	54.80	(55.16)
r_R	1.162	(1.172)	1.122	(1.13)	1.14	(1.139)
a_R	0.75	(0.75)	0.75	(0.75)	0.75	(0.75)
W_{vol}	3.74	(3.50)	3.0	(2.70)	3.0	(2.65)
r_{IM}	1.32	(1.32)	1.33	(1.33)	1.33	(1.33)
a_{IM}	0.66	(0.615)	0.696	(0.667)	0.672	(0.65)
W_{surf}	6.27	(6.11)	6.49	(6.72)	6.86	(7.09)
V_{LS}	6.20	(6.20)	6.4	(6.4)	6.1	(6.1)
r_{LS}	1.01	(1.01)	1.12	(1.12)	1.14	(1.125)
a_{LS}	0.75	(0.75)	0.75	(0.75)	0.75	(0.75)
X^2/N	1.4	(2.6)	1.4	(1.6)	1.1	(1.8)
$\sigma_{D+E}(2_1^+)$	0.215	(.212)	0.235	(.208)	0.229	(.203)
$\sigma_{D+E}(4_1^+)$	0.0674	(.0629)	0.0727	(.0613)	0.0717	(.0599)
$\sigma_{D+E}(6_1^+)$	0.0431	(.0256)	0.0456	(.0241)	0.0455	(.0237)

Table IV. Deformation lengths and transition strengths for ^{138}Ba and ^{144}Sm from this work.

^{138}Ba				^{144}Sm			
Ex Energy (keV)	J^{π}	$\beta_L R'$ (F)	G(L)	Ex Energy (keV)	J^{π}	$\beta_L R'$ (F)	G(L)
1436	2^+	0.43	6.1	1661	2^+	0.46	8.7
2218	2^+	0.23	1.7	2423	2^+	0.29	3.5
2639	2^+	0.07	0.2	2800	2^+	0.14	0.8
3339	2^+	0.15	0.7	1811	3^-	0.87	34.0
3368	2^+	0.17	1.0	3227	3^-	0.07	0.3
2881	3^-	0.73	18.9	2191	4^+	0.33	5.8
1898	4^+	0.31	4.1	2588	4^+	0.21	2.3
2308	4^+	0.21	1.9	2883	4^+	0.25	3.2
2584	4^+	0.08	0.2	3020	4^+	0.23	2.8
2779	4^+	0.12	0.6	2324	(6^+)	0.11[a] 0.18	1.0[a] 2.8
3156	4^+	0.07	0.2	3308	6^+	0.15	1.8
2090	6^+	0.30	6.3				
2201	(6^+)	0.15	1.7				

[a]These numbers represent the extreme credible fits to the data.

Table V. Summary of deformation lengths and G_L values for states in ^{138}Ba and ^{144}Sm from various reactions.

	J^π	E* [MeV]	Reaction	Beam Energy [MeV]	$\delta_L' = \beta_L' R'$ [F]	G_L	Reference
^{138}Ba	2^+	1.436	(p,p')	30	0.43	6.1	Present Work
	2^+	1.436	(α,α')	50	0.42	5.6	17
	4^+	1.898	(p,p')	30	0.31	4.1	Present Work
	4^+	1.898	(α,α')	50	0.30	3.6	17
	2^+	2.218	(p,p')	30	0.23	1.7	Present Work
	2^+	2.19	(α,α')	50	0.19	1.2	17
	4^+	2.308	(p,p')	30	0.21	1.9	Present Work
	4^+	2.27	(α,α')	50	0.19	1.4	17
	3^-	2.881	(p,p')	30	0.73	18.9	Present Work
	3^-	2.88	(α,α')	50	0.58	11.6	17
	2^+	3.339	(p,p')	30	0.15	0.7	Present Work
	(2^+)	3.34	(α,α')	50	0.18	1.0	17
^{144}Sm	2^+	1.661	(p,p')	30	0.46	8.7	Present Work
	2^+	1.66	(p,p')	30	0.44	7.4[a]	18
	2^+	1.659	(p,p')	50	0.41	6.4	19
	2^+	1.66	(^{3}He,^{3}He')	53	0.47	8.5	19
	2^+	1.66	(α,α')	50	0.43	7.0	18
	3^-	1.811	(p,p')	30	0.87	34.0	Present Work
	3^-	1.81	(p,p')	30	0.82	27.6[a]	18
	3^-	1.82	(^{3}He,^{3}He')	53	0.71	20.7	19
	3^-	1.81	(α,α')	50	0.71	20.8	18
	4^+	2.191	(p,p')	30	0.33	5.8	Present Work
	4^+	2.19	(p,p')	30	0.32	4.9[a]	18
	4^+	2.19	(α,α')	50	0.30	4.2	18
	2^+	2.423	(p,p')	30	0.29	3.5	Present Work
	2^+	2.45	(p,p')	30	0.29	3.2[a]	18
	2^+	2.45	(α,α')	50	0.26	2.5	18

[a]The quantities G_L listed in Ref. 18 for (p,p') are wrong due to an arithmetic error. The corrected values are given above. Private communication from J.H. Barker.

Table VI. Ratio of excitations below E_x=3.3 MeV by (p,p') in ^{138}Ba and ^{144}Sm.

J^π	2^+	3^-	4^+
$\frac{\sum_i G_i(^{144}\mathrm{Sm})}{\sum_i G_i(^{138}\mathrm{Ba})}$	1.35	1.81	2.02
$\frac{\sum_i E_i G_i(^{144}\mathrm{Sm})}{\sum_i E_i G_i(^{138}\mathrm{Ba})}$	1.36	1.14	2.44

Table VII. Effective charges for transitions in ^{138}Ba.

Transition	L[b]	δe[c]
$0^+ \rightarrow 2_1^+$	2	0.82±0.23
$0^+ \rightarrow 4_1^+$	4	0.86±0.23
$0^+ \rightarrow 6_1^+$	6	0.61±0.23
$0^+ \rightarrow 2_2^+$	2	0.98±0.23
$0^+ \rightarrow 4_2^+$	4	1.07±0.23
$0^+ \rightarrow (6_2^+)$[a]	6	0.73±0.23

[a]This state has not been unambiguously assigned 6^+, but its angular distribution, together with the shell-model predictions, suggest this assignment.

[b]This is the L-transfer for the dominant amplitude. Non-normal parity amplitudes also contribute to the cross section, and are included in the calculations. See Ref. 25.

[c]Calculated from the relationship $[(1+\delta e(1+2N/Z)]^2=\sigma_{exp}/\sigma_{theory}$ where the theoretical cross section σ_{theory} is calculated using the shell model wave functions described in the text.

Table VIII. Major components of 0_1^+ and 6_2^+ wave functions[a] calculated with both interactions, and the resulting matrix elements for the associated transition densities.

$|0^+\rangle_{g.s.} = -0.675|(g_7)^6\rangle - 0.674|(g_7)^4(d_5)^2\rangle - 0.286|(g_7)^2(d_5)^4\rangle$: A=136-140

$|0^+\rangle_{g.s.} = -0.517|(g_7)^6\rangle - 0.740|(g_7)^4(d_5)^2\rangle - 0.419|(g_7)^2(d_5)^4\rangle$: A=136-145

$|6_2^+\rangle = 0.599|(g_7)^6\rangle - 0.559|(g_7)^5(d_5)^1\rangle - 0.318|(g_7)^3(d_5)^3\rangle - 0.316|(g_7)^4(d_5)^2\rangle$: A=136-140

$|6_2^+\rangle = 0.573|(g_7)^6\rangle - 0.303|(g_7)^5(d_5)^1\rangle - 0.246|(g_7)^3(d_5)^3\rangle - 0.621|(g_7)^4(d_5)^2\rangle$: A=136-145

	$M^0_{606}(g_{7/2},g_{7/2})$	$M^0_{606}(g_{7/2},d_{5/2})$	$M^0_{606}(d_{5/2},g_{7/2})$
A = 136-140	0.1292	0.1049	0.2174
A = 136-145	0.1765	0.0800	0.1178

[a]The subscripts on the single particle orbitals are 2*j i.e. $g_{7/2} \equiv g_7$.

Table IX. Comparison of D[a] and D+E[b] cross sections for various interactions in ^{138}Ba.

Interaction[c]	2_1^+ D	2_1^+ D+E	4_1^+ D	4_1^+ D+E	6_1^+ D	6_1^+ D+E	$\frac{4^+ D+E}{2^+ D+E}$	$\frac{6^+ D+E}{2^+ D+E}$
CAL	.00994	0.299	.00417	0.170	0.00562	0.195	0.569	0.652
COP	3.456	0.936	0.846	0.241	0.343	0.460	0.257	0.491
CE-I	0.357	1.832	0.0921	0.818	0.0489	0.767	0.447	0.419
F-V	0.268	0.191	0.0691	0.191	0.0357	0.334	1.00	1.749
ROSENFELD	0.437	0.166	0.110	0.166	0.0517	0.320	1.00	1.928
SOPER	1.360	1.584	0.330	0.426	0.129	0.210	0.269	0.133
SERBER	2.135	3.691	0.521	1.196	0.210	0.777	0.324	0.211

[a]Includes only direct amplitudes.

[b]Includes both direct and knock-on exchange amplitudes.

[c]Summarized in Ref. 61.

FIGURE CAPTIONS

Figure 1. Slit and counter arrangement of high resolution measurement-optimization-stabilization system located in the focal plane of the spectrograph. The experimental parameters are adjusted until the maximum amount of elastically scattered beam passes between the brass jaws, thus insuring minimum line widths of the groups of scattered particles along the focal plane.

Figure 2. Spectrum of $^{138}Ba(p,p')$ at 35 degrees, with resolution of about 10 keV, FWHM. The broad bumps correspond to protons which scatter from Mg and Si impurities and because of kinematic differences have different planes of focus in the spectrograph. The yields of the 2^+ state at 1436 keV and of the 3^- state at 2881 keV were too intense to be counted on this plate. The height of the peak corresponding to the 1.898 MeV state is 1675 counts.

Figure 3. Spectrum from $^{144}Sm(p,p')$ at 40 degrees, with resolution of about 7 keV, FWHM. The broad bumps under certain of the peaks correspond to protons which scatter from Mg and Si impurities, as in the ^{138}Ba spectrum. The yield of the 3^- state at 1811 keV was too intense to be counted on this plate. To the right of channel 454, the counts per channel have been multiplied by 5.

Figure 4. Elastic scattering angular distributions measured for ^{138}Ba and ^{144}Sm. The curves are results of optical model calculations made with the optical model parameters of Becchetti and Greenlees (Ref. 37).

Figure 5. Characteristic curves obtained by averaging our measured angular distributions from groups of states in ^{138}Ba and ^{144}Sm which had previously assigned J^{π} values.

Figure 6. States in ^{138}Ba which have angular distributions in agreement with the characteristic 2^+ shape, which is the line drawn through the data. We assign all of these states $J^{\pi}=2^+$ with the exception of the state at 3050 keV.

Figure 7. States in ^{144}Sm which have angular distributions in agreement with the characteristic 2^+ shape, which is the line drawn through the data. We assign all of these states $J^{\pi}=2^+$.

Figure 8. States in ^{138}Ba and ^{144}Sm which have angular distributions in agreement with the characteristic 3^- shape, which is the line drawn through the data. We assign these states $J^{\pi}=3^-$.

Figure 9. States in ^{138}Ba which have angular distributions in agreement with the characteristic 4^+ shape, which is the line drawn through the data. We assign all of these states $J^{\pi}=4^+$.

Figure 10. States in ^{144}Sm which have angular distributions in agreement with the characteristic 4^+ shape, which is the line drawn through the data. We assign all of these states $J^\pi=4^+$.

Figure 11. Angular distributions for the previously assigned 6^+ state at 2090 keV, and the weak 2201 keV member of a doublet in ^{138}Ba. Both the 4^+ and 6^+ characteristic curves are drawn through this angular distribution. The 2324 keV state in ^{144}Sm has been assigned 6^+, but due to the rise of the data at forward angles, this state may be a close lying doublet. We assign $J^\pi=6^+$ to the 3308 keV state in ^{144}Sm.

Figure 12. Angular distributions of states in ^{138}Ba for which no J^π assignment could be made from this work. Spins of 5^+ and 3^+ have been suggested for the states at 2415 and 2445 keV respectively (Ref. 40).

Figure 13. Angular distributions of states in ^{144}Sm for which no J^π assignment could be made from this work. The state at 3123 keV has been assigned $J^\pi=7^{\pm}$ in Ref. 11.

Figure 14. Comparison of results of shell model calculations discussed in Sec. IVA with experimentally known energy levels in ^{138}Ba.

Figure 15. Comparison of results of shell model calculations discussed in Sec. IVA with experimentally known energy levels in ^{144}Sm.

Figure 16. Results of collective model calculations for inelastic scattering on ^{138}Ba. The optical model parameters given in Table III, Set SII were used, and both the real and imaginary parts of the optical model were deformed. The calculations shown are for the lowest 2^+, 3^-, 4^+, and 6^+ states.

Figure 17. Results of collective model calculations for inelastic scattering on ^{144}Sm. The optical model parameters given in Table III, Set SI were used, and both the real and imaginary parts of the optical model were deformed. The calculations shown are for the lowest 2^+, 3^-, 4^+, and 6^+ states.

Figure 18. Microscopic model DWBA calculations for the inelastic scattering to the 2^+_1, 4^+_1, and 6^+_1 states in ^{138}Ba. The calculations are identical except for the wave functions; the left hand column employed the A=136-140 set while the A=136-145 set was used for the right hand column. Both sets of wave functions predict very similar angular distributions. The cross section enhancement factor was calculated for δe=0.8.

Figure 19. Microscopic model DWBA calculations for the inelastic scattering to the 2_2^+, 4_2^+, and 6_2^+ states in ^{138}Ba. The calculations are identical except for the wave functions; the left hand column employed the A=136-140 set while the A=136-145 set was used for the right hand column. These calculations indicate that the A=136-140 set of wave functions provides the better description of the low-lying states in ^{138}Ba. The cross section enhancement factor was calculated for δ_e=0.8.

Figure 20. Transition densities for the $2_{1,2}^+$, $4_{1,2}^+$, and $6_{1,2}^+$ states in ^{138}Ba calculated with both sets of wave functions. The 2_1^+, 4_1^+, and 6_1^+ densities are very similar, and predict very similar cross sections. The differences in the 2_2^+, 4_2^+, and 6_2^+ cross sections are directly related to the differences in the transition densities for these states.

Figure 21. Composition of the 6_2^+ transition density in ^{138}Ba, calculated with both sets of wave functions. The left hand figure is calculated with the A=136-140 set while the right hand figure is calculated with the A=136-145 set. The unlabeled line is the total transition density, the sum of the other two curves.

Figure 22. Microscopic model DWBA calculations for inelastic scattering to the 3_1^+ and 5_1^+ states in ^{138}Ba calculated with the A=136-140 set of wave functions. The two-body force included central, tensor and L-S terms, but no collective renormalization was included. Only the Direct + Exchange calculations are shown.

Figure 23. Microscopic model DWBA calculations for inelastic scattering to the $2_{1,2}^+$, $4_{1,2}^+$, and $6_{1,2}^+$ states in ^{144}Sm calculated with the A=136-145 set of wave functions. The inadequacy of the basis space is demonstrated in the calculated angular distributions for the 2_2^+, 4_2^+, and 6_2^+ states. The cross section enhancement factor was calculated with $\delta e=0.8$.

DETECTOR SETUP — ELASTIC PEAK

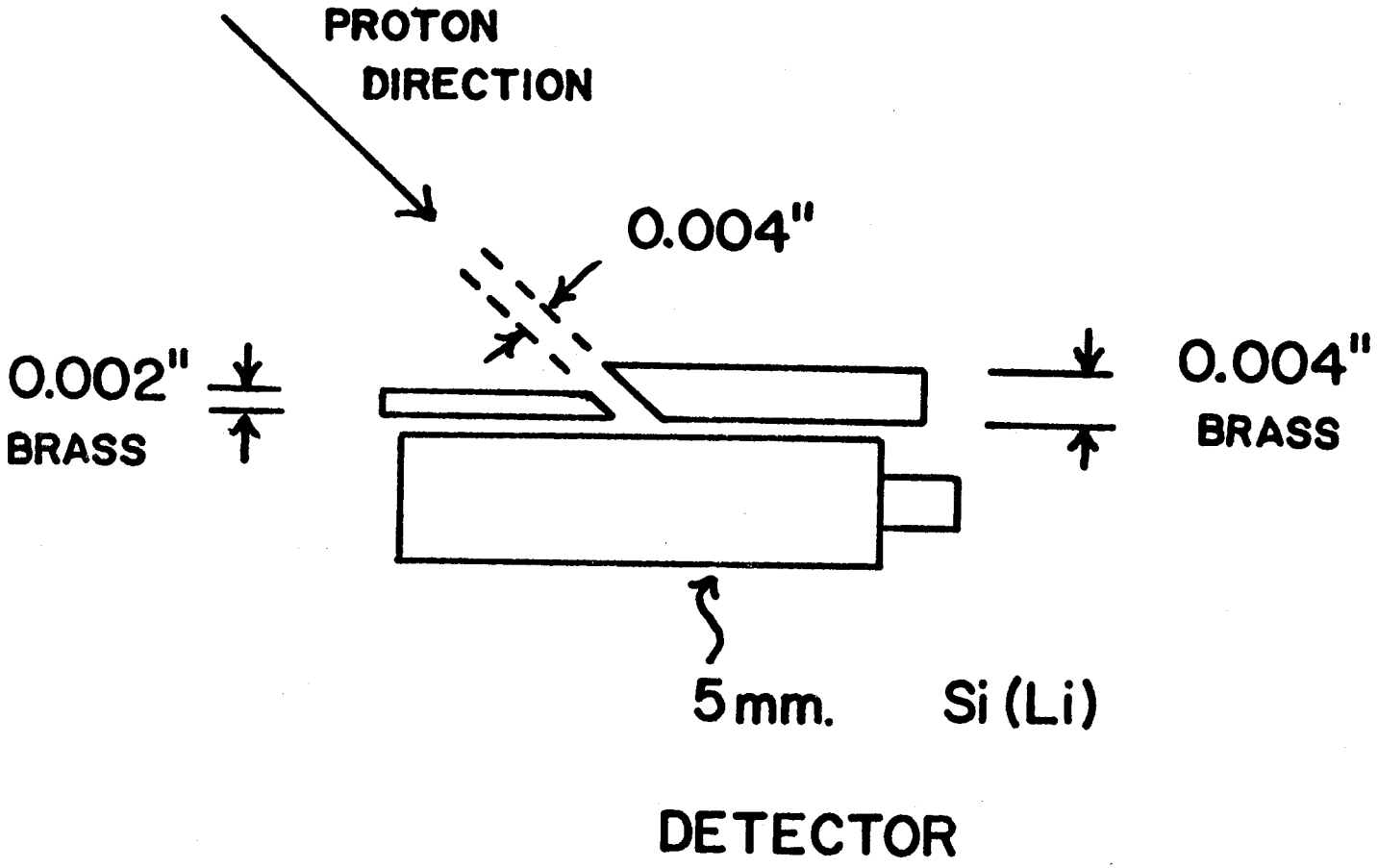

MSUCL

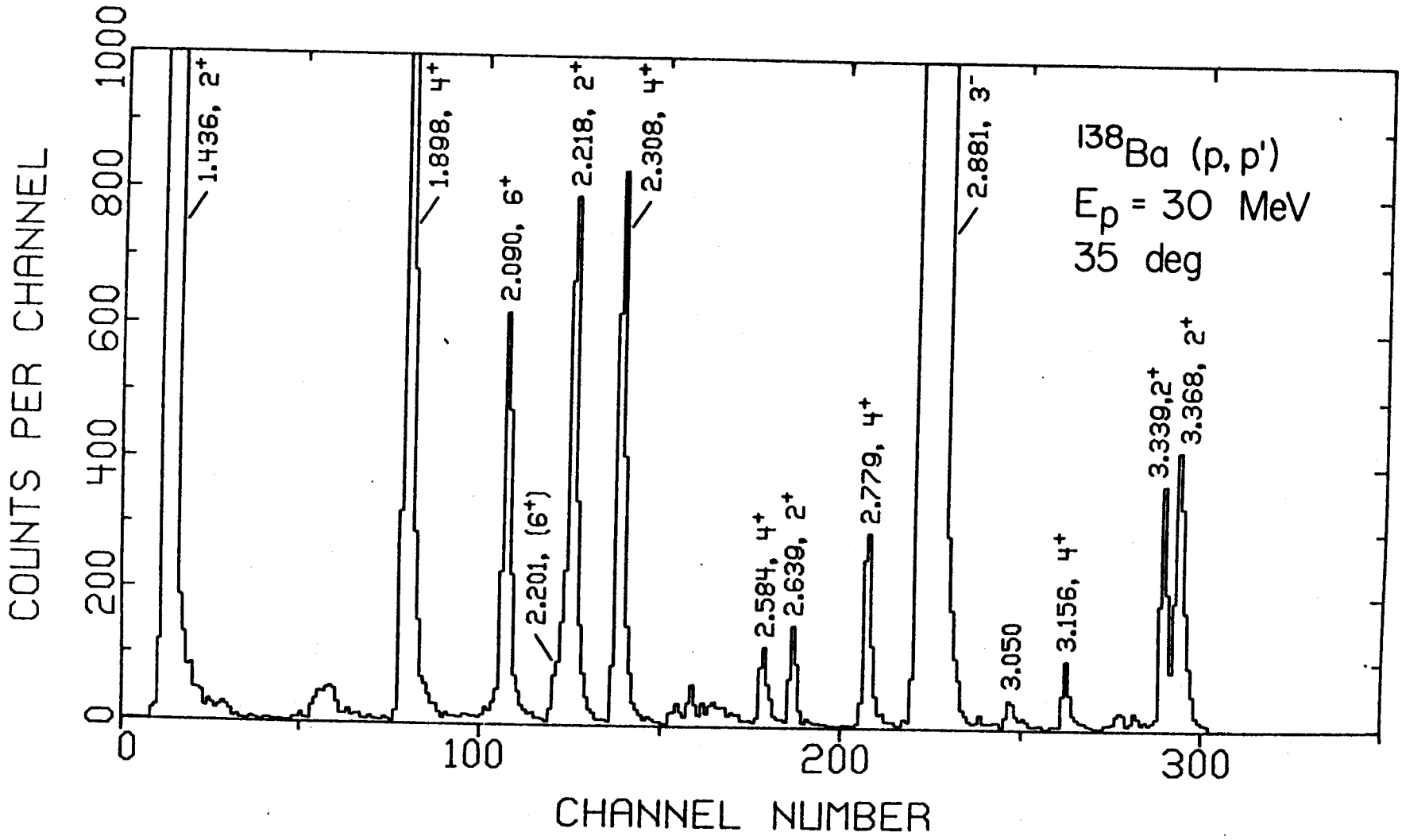
COUNTS PER CHANNEL
0
200
400
600
800
1000
0
100
200
300
CHANNEL NUMBER
1.436, 2+
1.898, 4+
2.090, 6+
2.201, (6+)
2.218, 2+
2.308, 4+
2.584, 4+
2.639, 2+
2.779, 4+
2.881, 3-
3.050
3.156, 4+
3.339, 2+
3.368, 2+
138Ba (p, p')
Ep = 30 MeV
35 deg

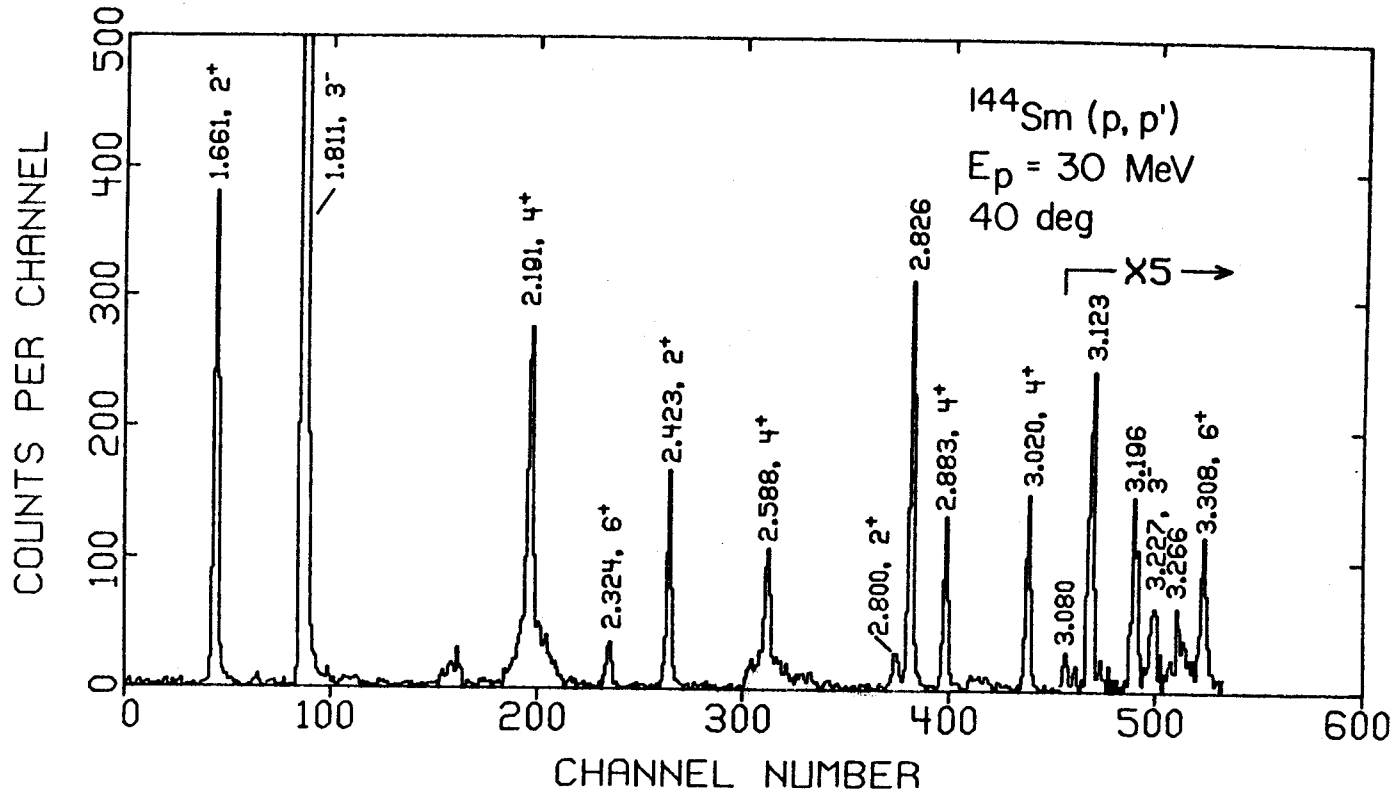
COUNTS PER CHANNEL
CHANNEL NUMBER
0
100
200
300
400
500
600
1.661, 2+
1.811, 3-
2.191, 4+
2.324, 6+
2.423, 2+
2.588, 4+
2.800, 2+
2.826
2.883, 4+
3.020, 4+
3.080
3.123
3.196
3.227, 3-
3.266
3.308, 6+
144Sm (p, p')
Ep = 30 MeV
40 deg
X5

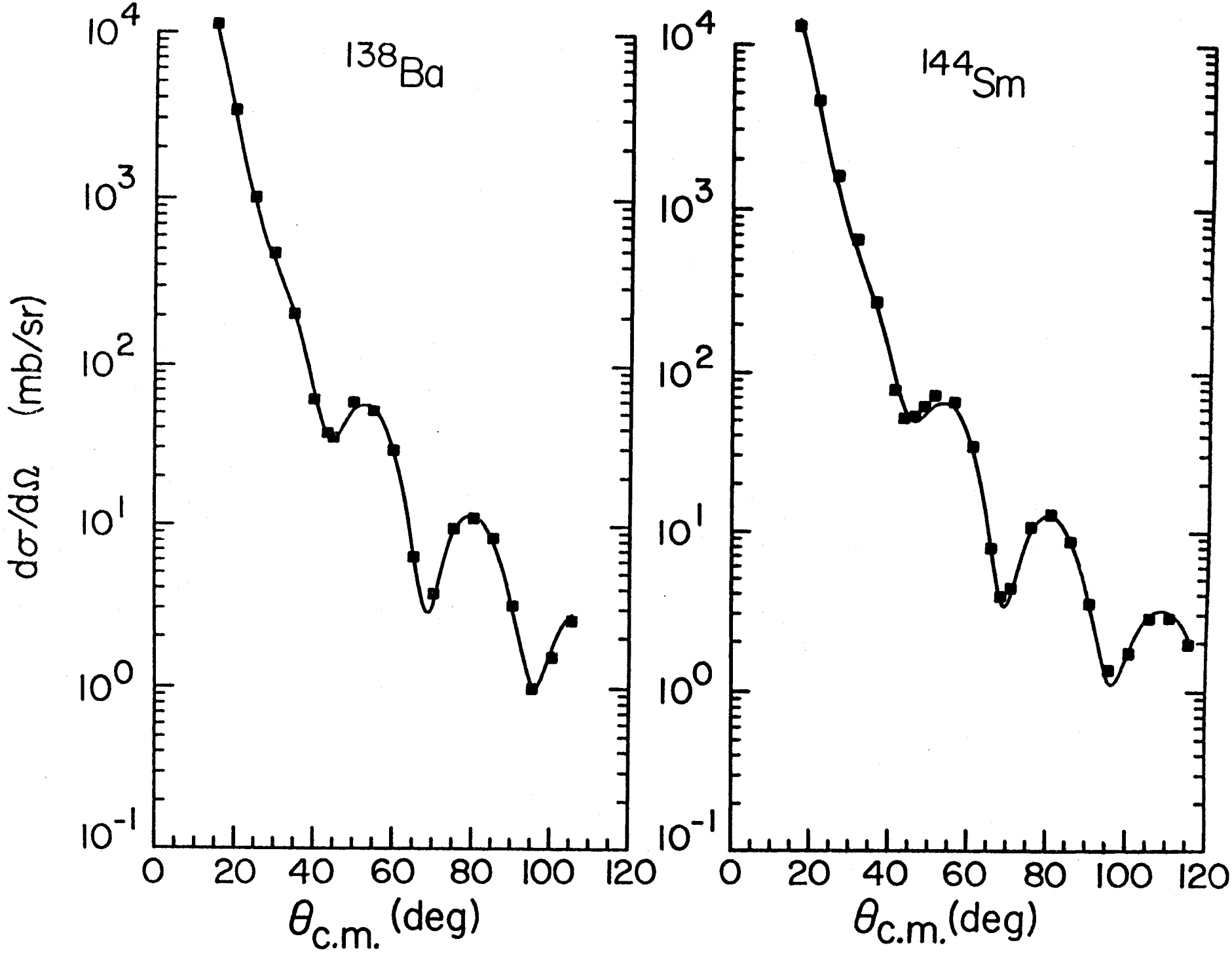
^{138}Ba
^{144}Sm
$d\sigma/d\Omega$ (mb/sr)
10^4
10^3
10^2
10^1
10^0
10^{-1}
0 20 40 60 80 100 120
$\theta_{c.m.}$ (deg)

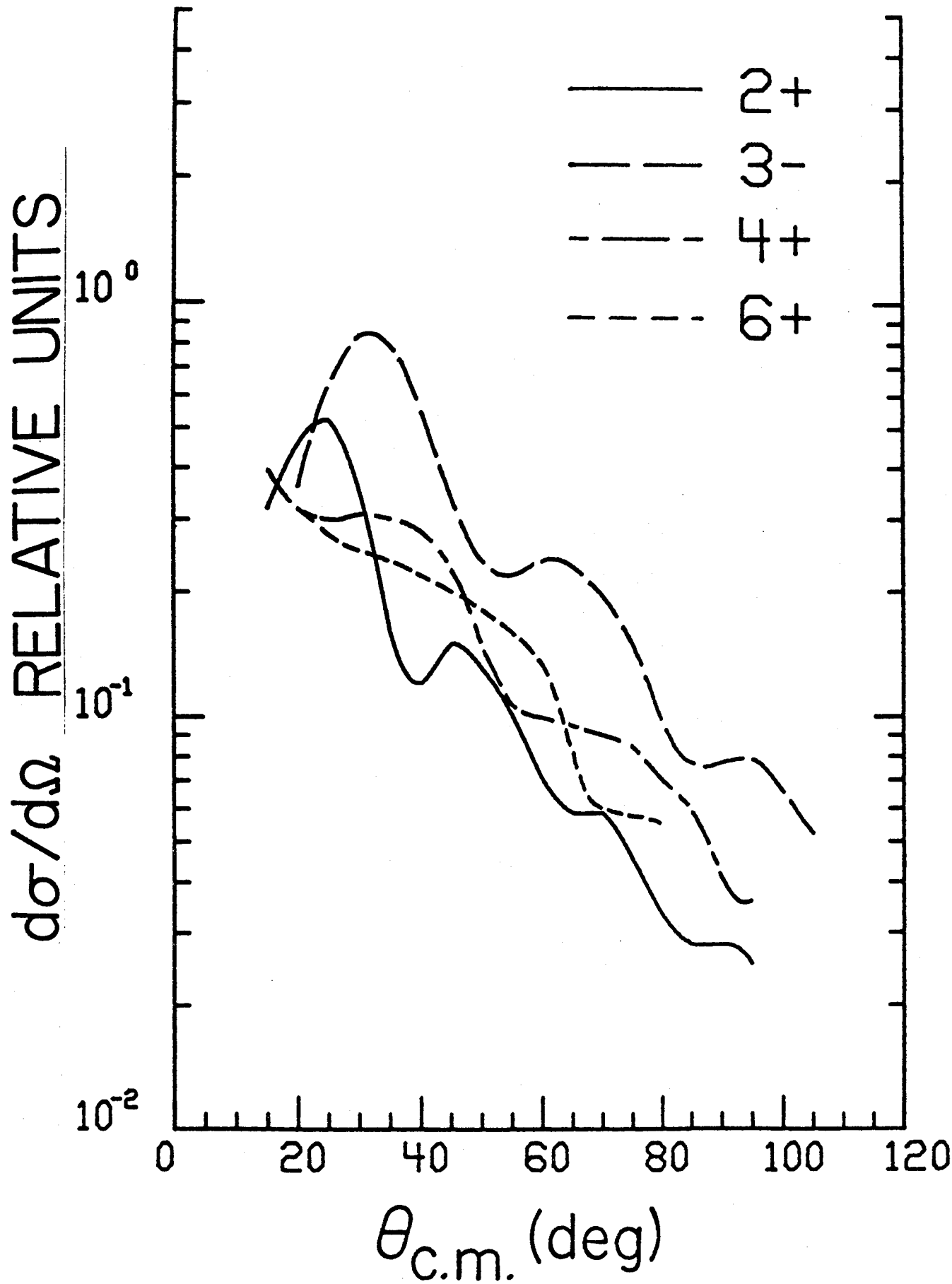
2+
3-
4+
6+
dσ/dΩ RELATIVE UNITS
10⁰
10⁻¹
10⁻²
0
20
40
60
80
100
120
θc.m. (deg)

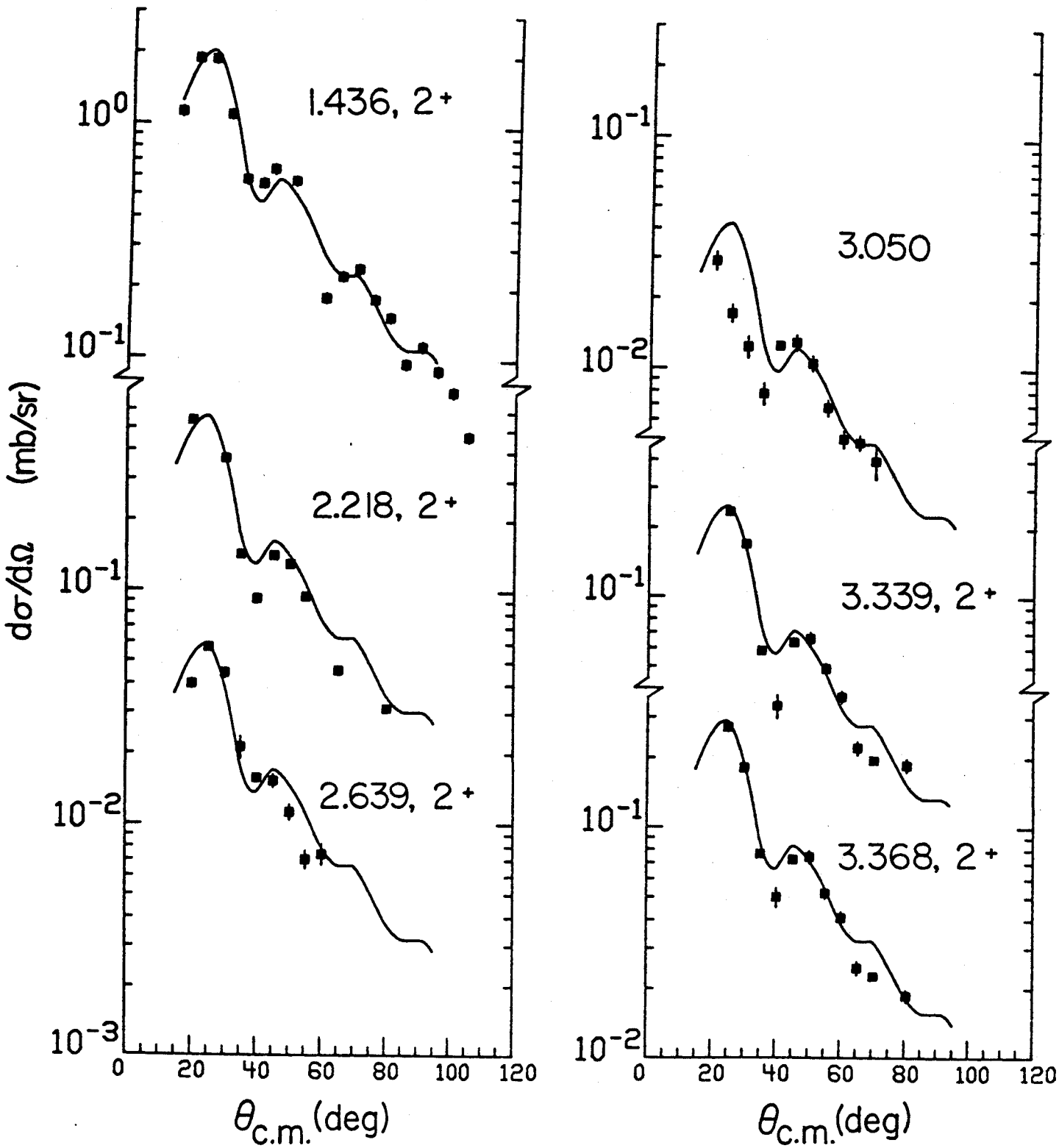
1.436, 2+
2.218, 2+
2.639, 2+
3.050
3.339, 2+
3.368, 2+
dσ/dΩ (mb/sr)
θc.m.(deg)
θc.m.(deg)

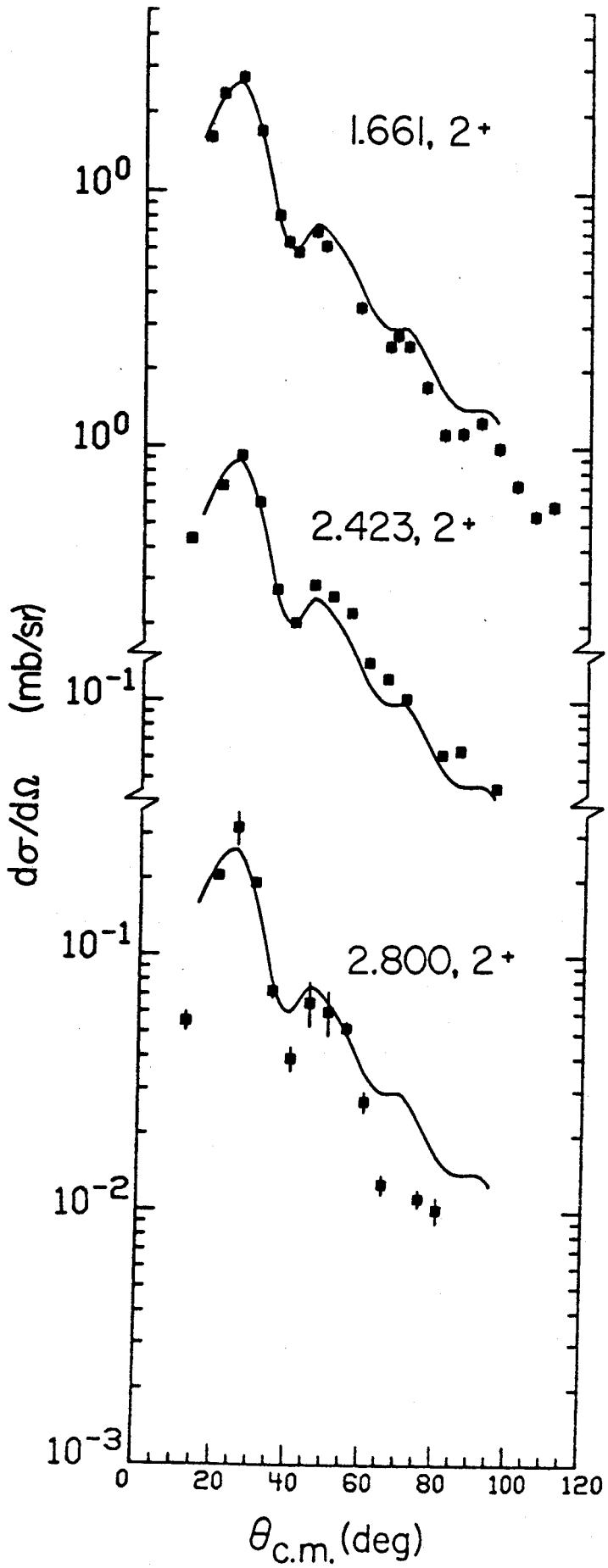
1.661, 2+
2.423, 2+
2.800, 2+
10^0
10^0
10^-1
10^-1
10^-2
10^-3
dσ/dΩ (mb/sr)
0
20
40
60
80
100
120
θc.m. (deg)

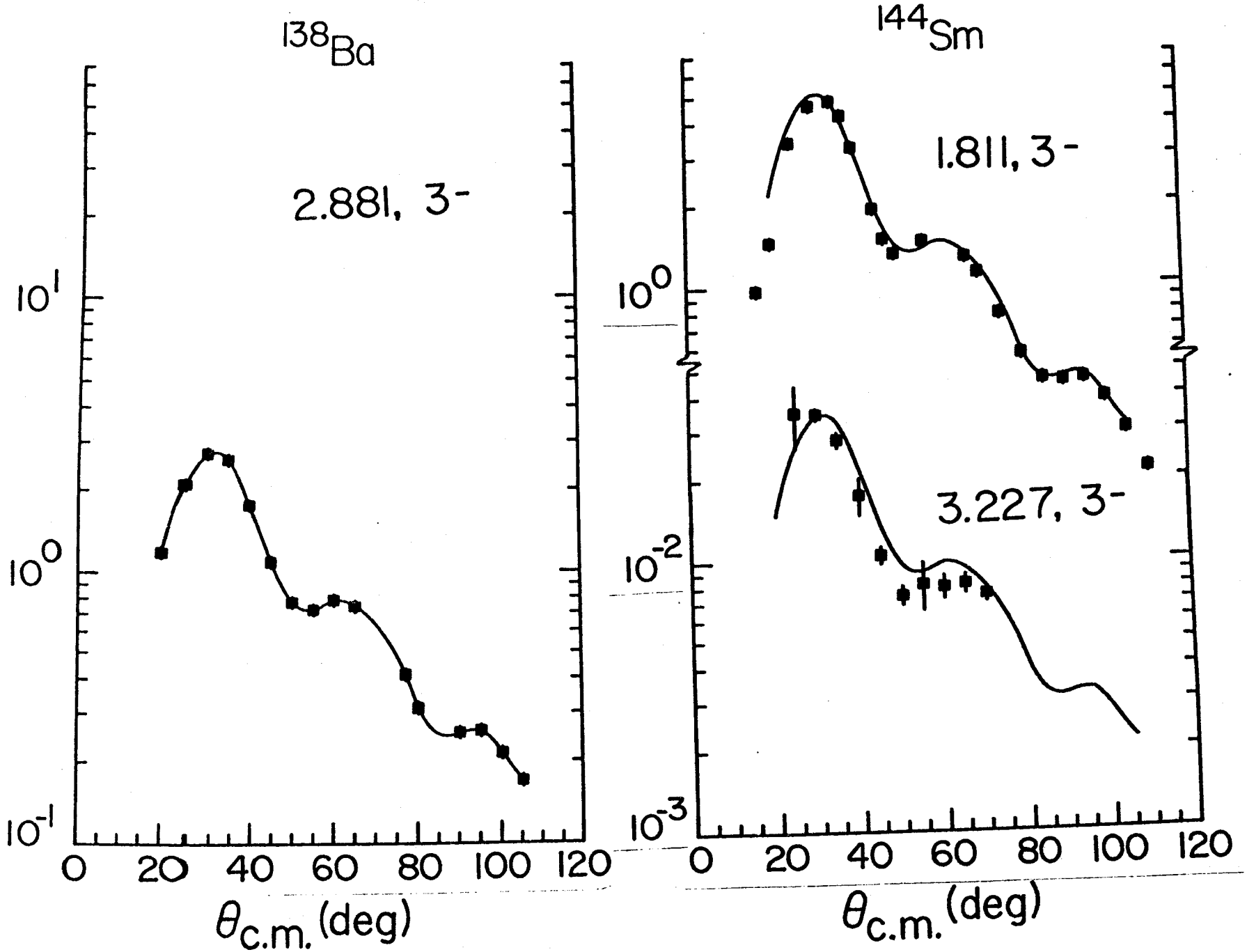
^{138}Ba
2.881, 3$^-$
10^1
10^0
10^{-1}
0 20 40 60 80 100 120
$\theta_{c.m.}$ (deg)
^{144}Sm
1.811, 3$^-$
3.227, 3$^-$
10^0
10^{-2}
10^{-3}
0 20 40 60 80 100 120
$\theta_{c.m.}$ (deg)

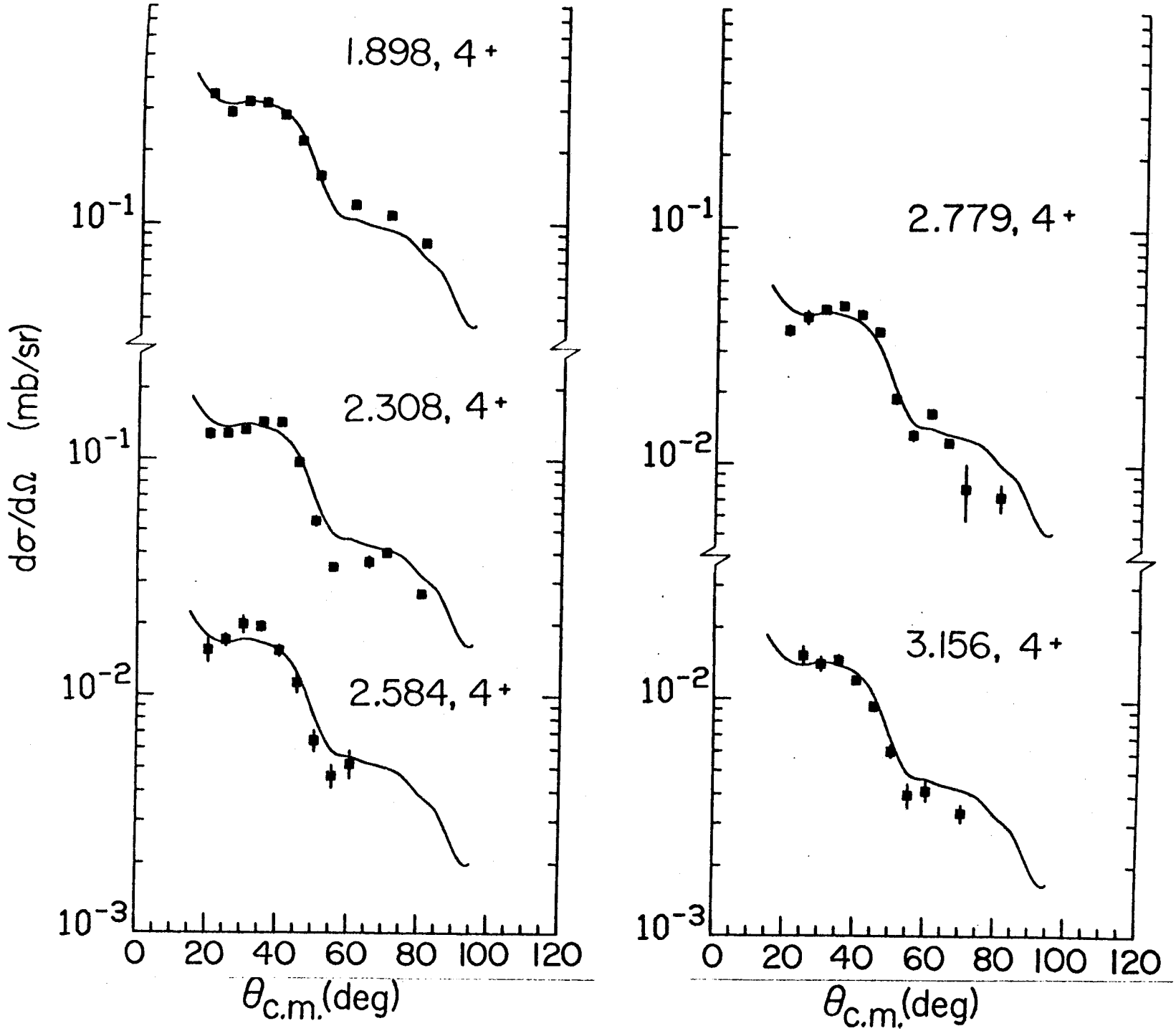
1.898, 4+
2.308, 4+
2.584, 4+
2.779, 4+
3.156, 4+
dσ/dΩ (mb/sr)
10^-1
10^-2
10^-3
0 20 40 60 80 100 120
θc.m.(deg)

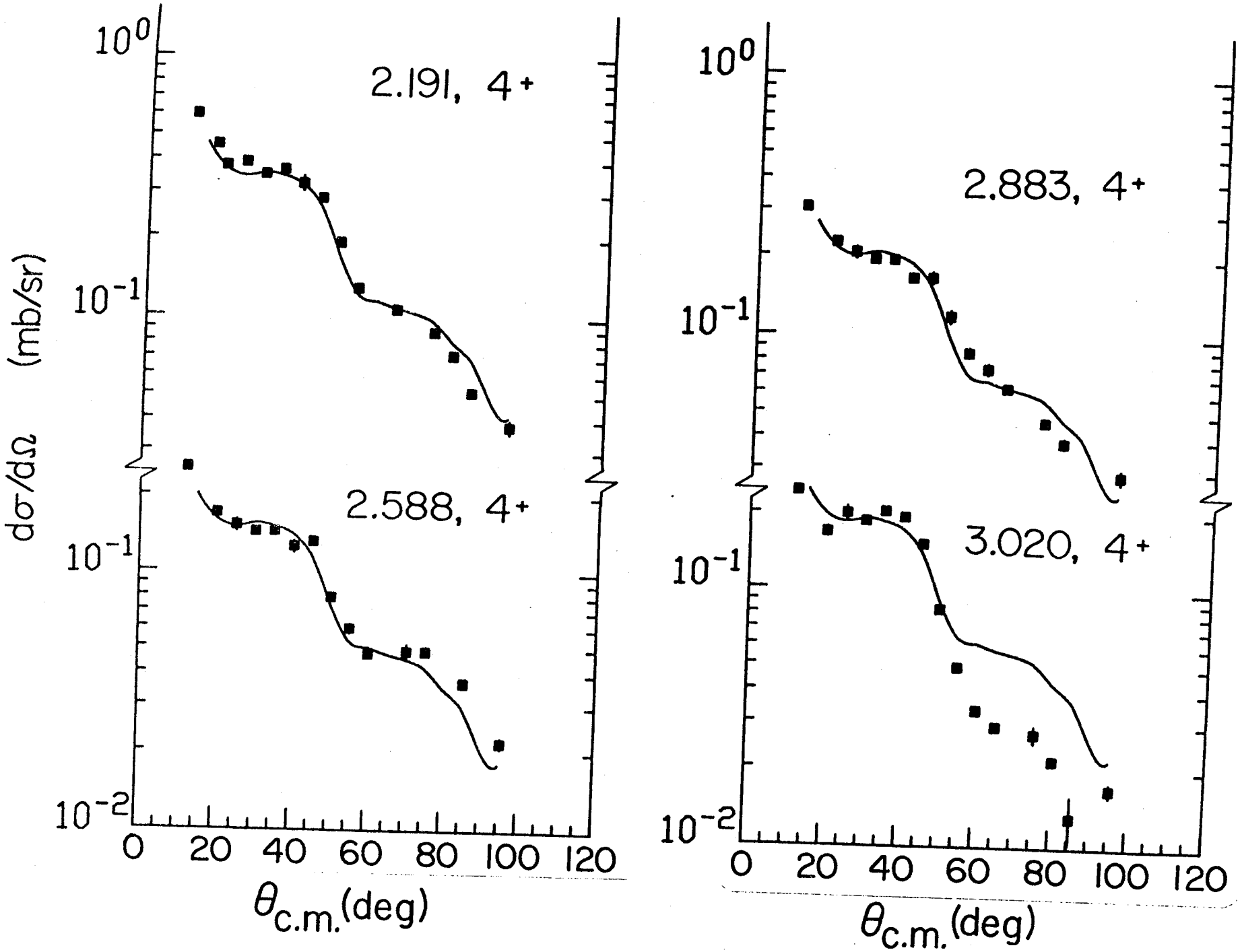
2.191, 4+
2.588, 4+
2.883, 4+
3.020, 4+
dσ/dΩ (mb/sr)
θc.m.(deg)
θc.m.(deg)

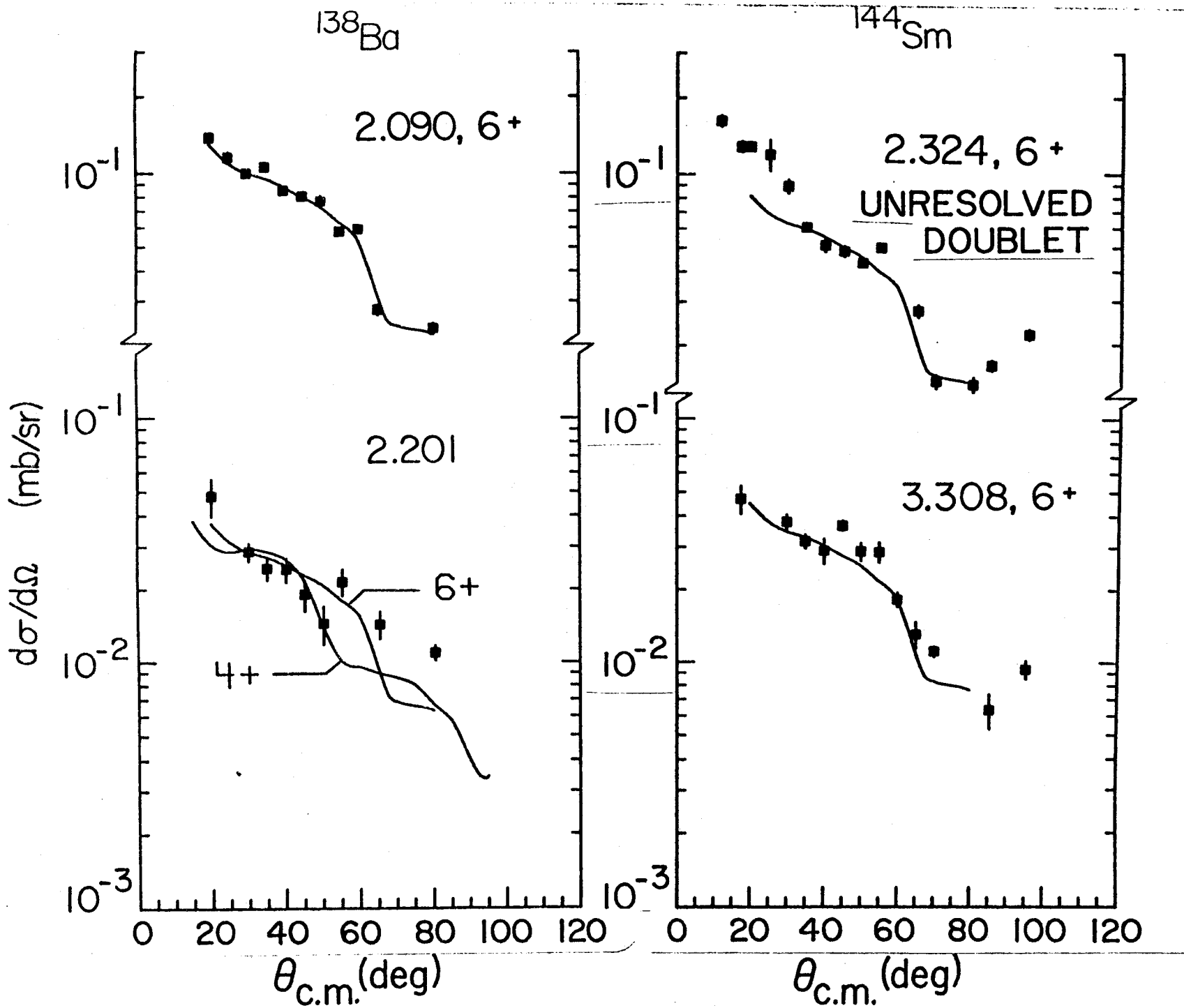
^{138}Ba
^{144}Sm
2.090, 6+
2.201
6+
4+
2.324, 6+
UNRESOLVED
DOUBLET
3.308, 6+
$d\sigma/d\Omega$ (mb/sr)
10^{-1}
10^{-2}
10^{-3}
0 20 40 60 80 100 120
$\theta_{c.m.}$(deg)

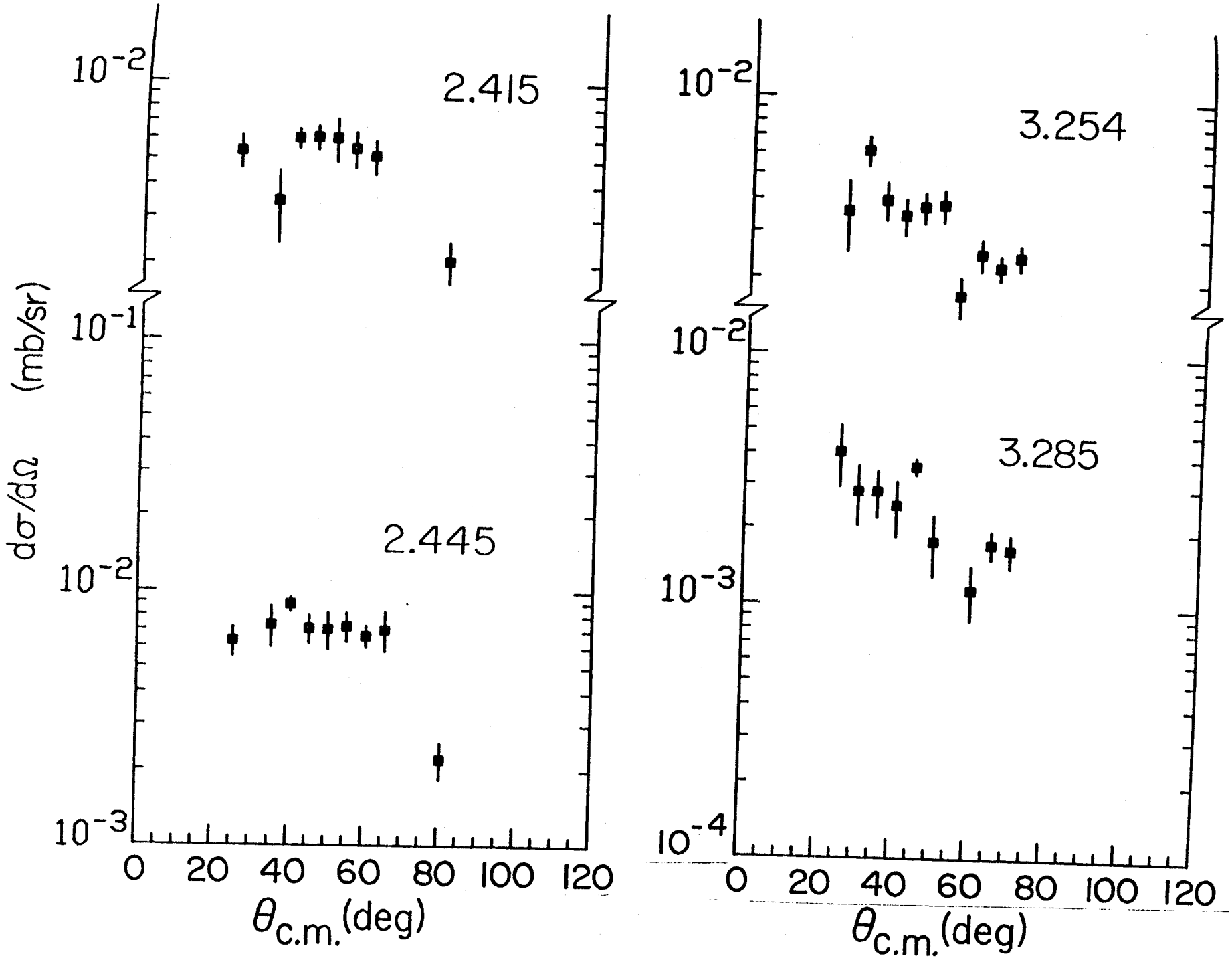
2.415
2.445
3.254
3.285
$d\sigma/d\Omega$ (mb/sr)
$\theta_{c.m.}$(deg)
$\theta_{c.m.}$(deg)

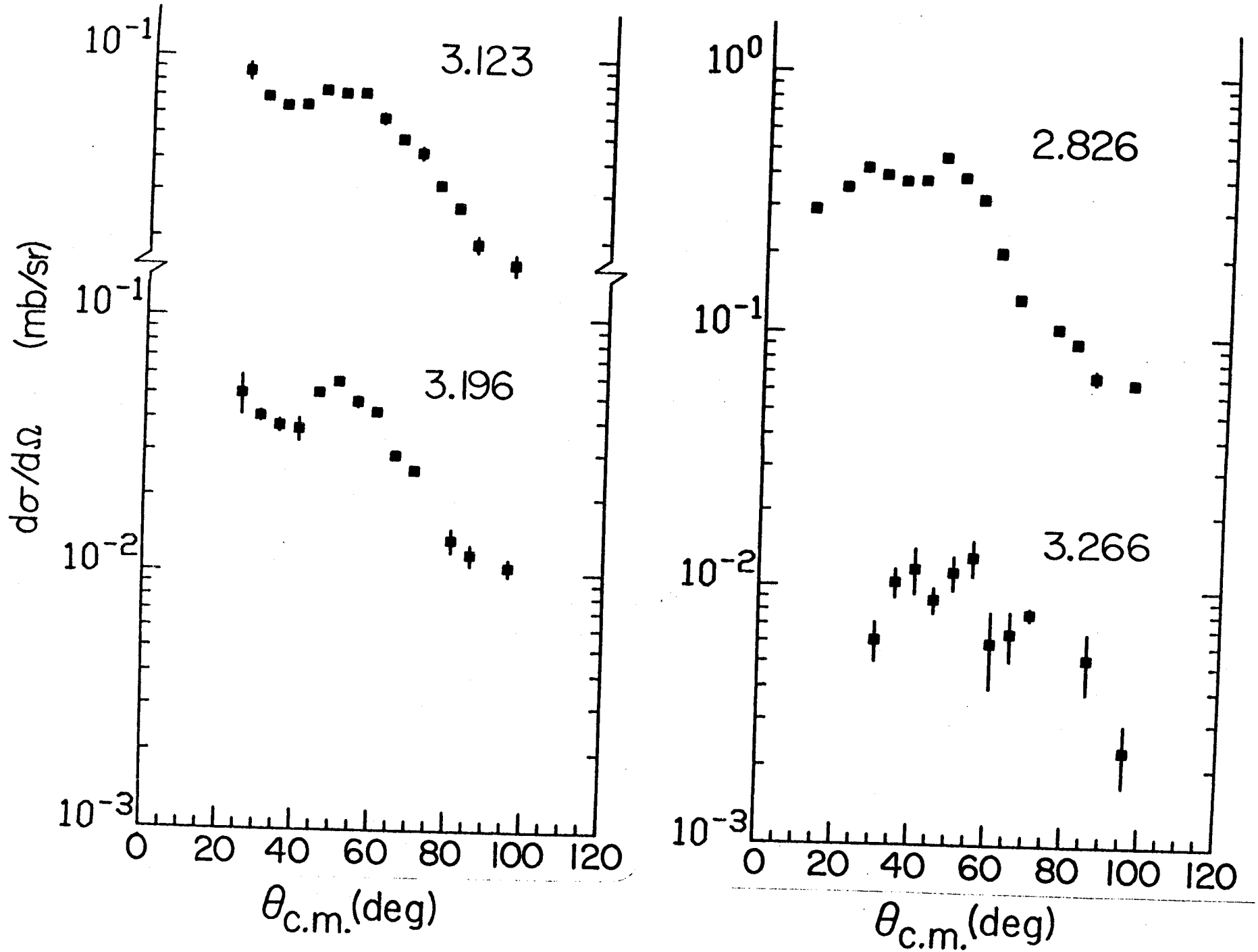
10^{-1}
10^{-1}
10^{-2}
10^{-3}
3.123
3.196
$d\sigma/d\Omega$ (mb/sr)
0 20 40 60 80 100 120
$\theta_{c.m.}$(deg)
10^{0}
10^{-1}
10^{-2}
10^{-3}
2.826
3.266
0 20 40 60 80 100 120
$\theta_{c.m.}$(deg)

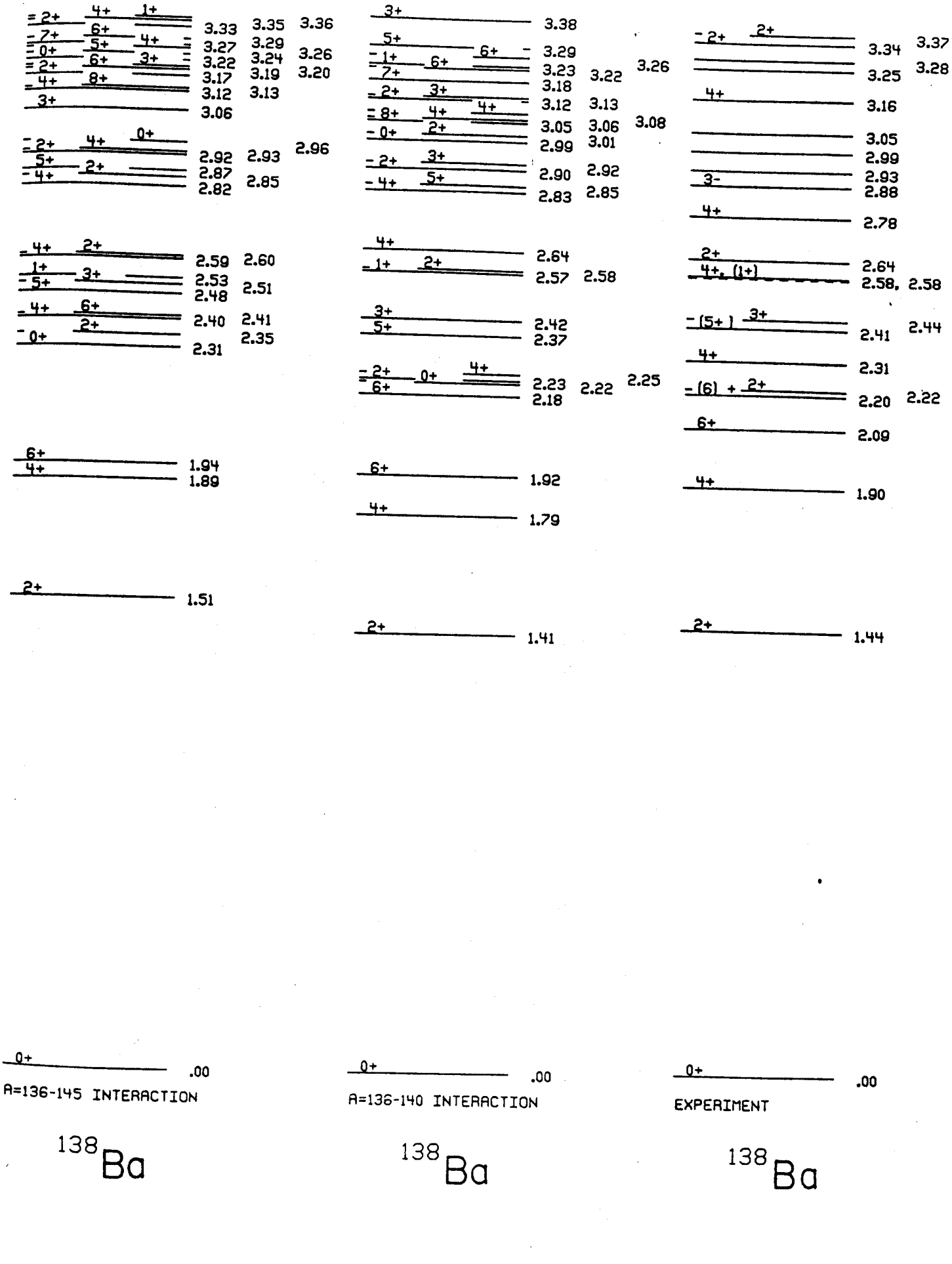
2+ 4+ 1+ 3.33 3.35 3.36
7+ 6+ 4+ 3.27 3.29
0+ 5+ 6+ 3+ 3.22 3.24 3.26
2+ 3.17 3.19 3.20
4+ 8+ 3.12 3.13
3+ 3.06
2+ 4+ 0+ 2.92 2.93 2.96
5+ 2+ 2.87
4+ 2.82 2.85
4+ 2+ 2.59 2.60
1+ 3+ 2.53
5+ 2.48 2.51
4+ 6+ 2.40 2.41
2+ 2.35
0+ 2.31
6+ 1.94
4+ 1.89
2+ 1.51
0+ .00
A=136-145 INTERACTION
138Ba
3+ 3.38
5+ 6+ 3.29
1+ 6+ 3.23 3.22 3.26
7+ 3.18
2+ 3+ 3.12 3.13
8+ 4+ 4+ 3.05 3.06 3.08
0+ 2+ 2.99 3.01
2+ 3+ 2.90 2.92
4+ 5+ 2.83 2.85
4+ 2.64
1+ 2+ 2.57 2.58
3+ 2.42
5+ 2.37
2+ 0+ 4+ 2.23 2.22 2.25
6+ 2.18
6+ 1.92
4+ 1.79
2+ 1.41
0+ .00
A=136-140 INTERACTION
138Ba
2+ 2+ 3.34 3.37
3.25 3.28
4+ 3.16
3.05
2.99
3- 2.93
2.88
4+ 2.78
2+ 2.64
4+, (1+) 2.58, 2.58
(5+) 3+ 2.41 2.44
4+ 2.31
(6) + 2+ 2.20 2.22
6+ 2.09
4+ 1.90
2+ 1.44
0+ .00
EXPERIMENT
138Ba

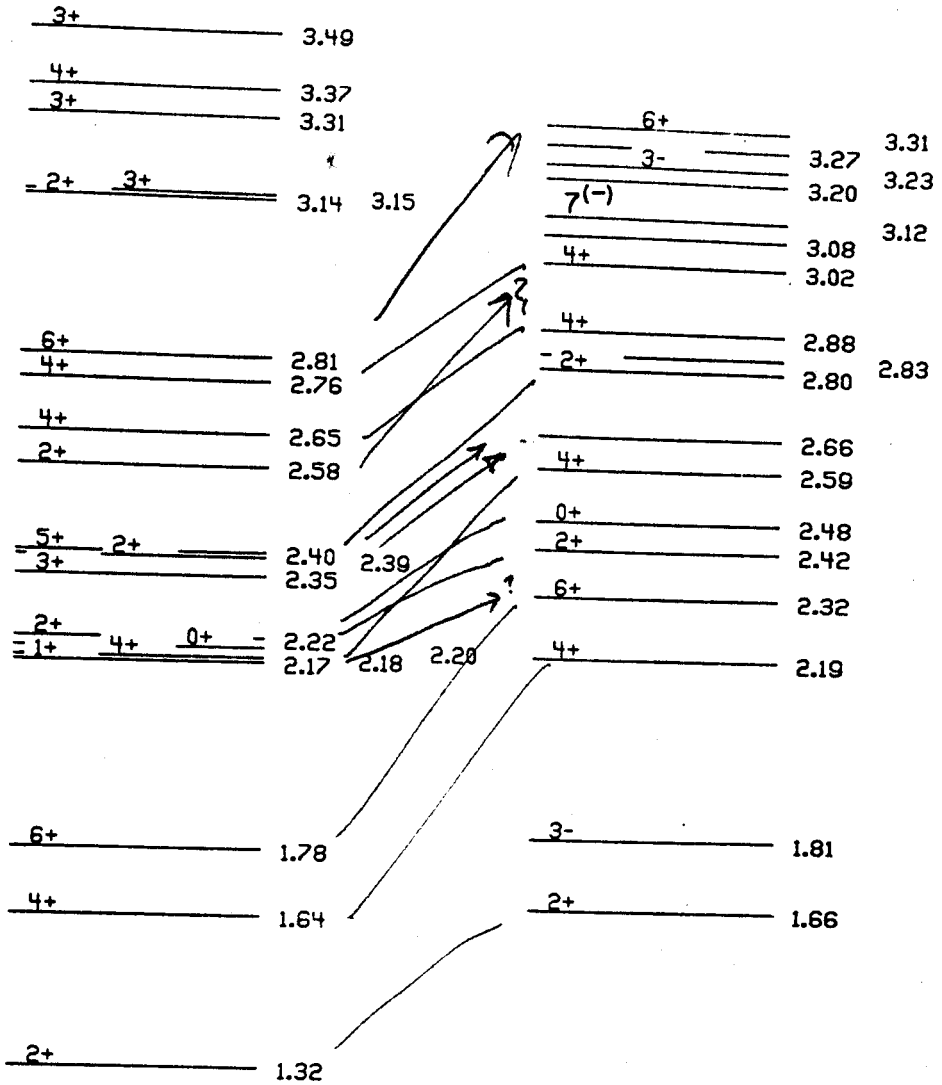

0+ .00

A=136-145 INTERACTION

^{144}Sm

0+ .00

EXPERIMENT

^{144}Sm

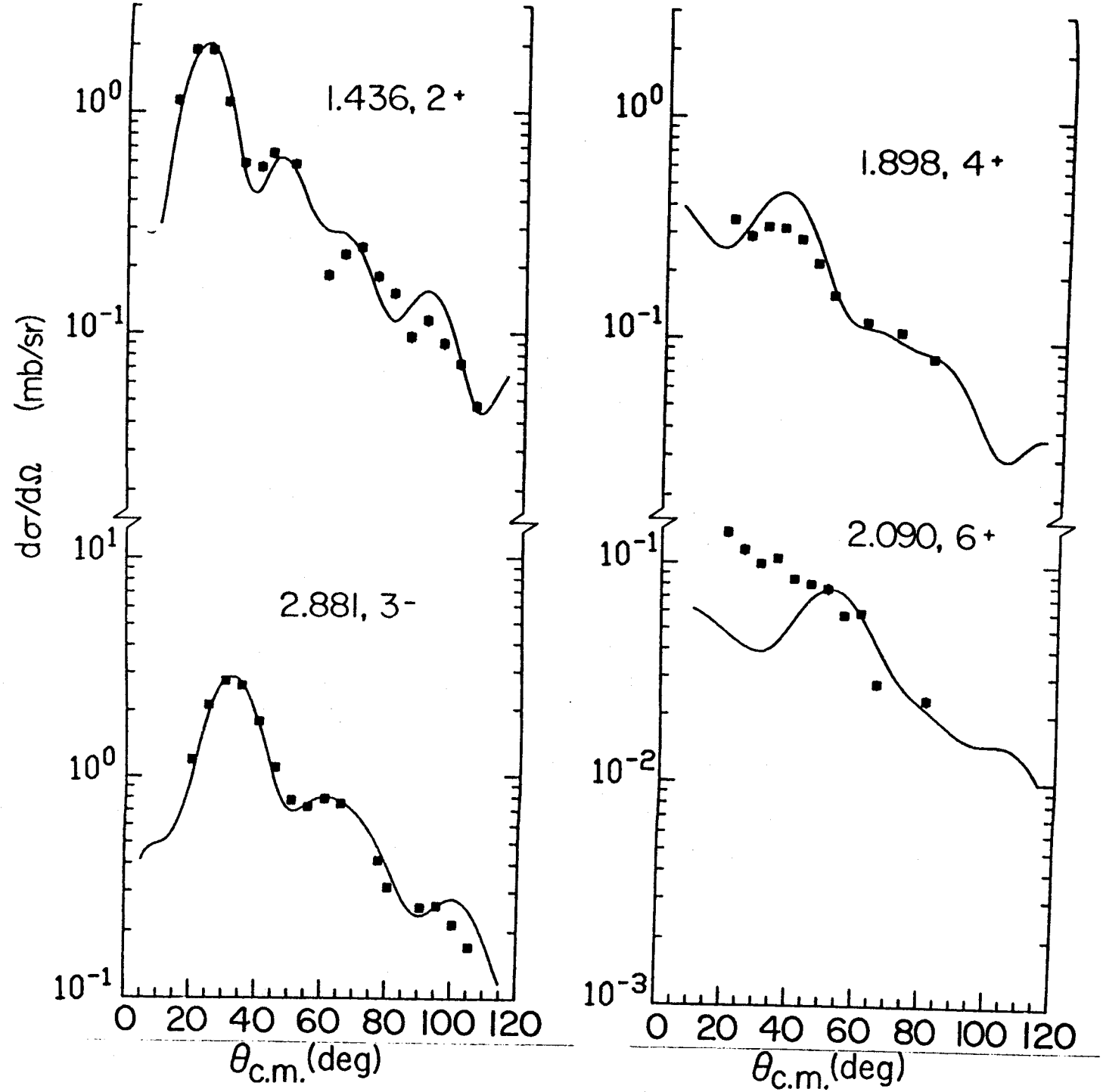
1.436, 2+
2.881, 3-
1.898, 4+
2.090, 6+
dσ/dΩ (mb/sr)
θc.m.(deg)
θc.m.(deg)
0 20 40 60 80 100 120
0 20 40 60 80 100 120

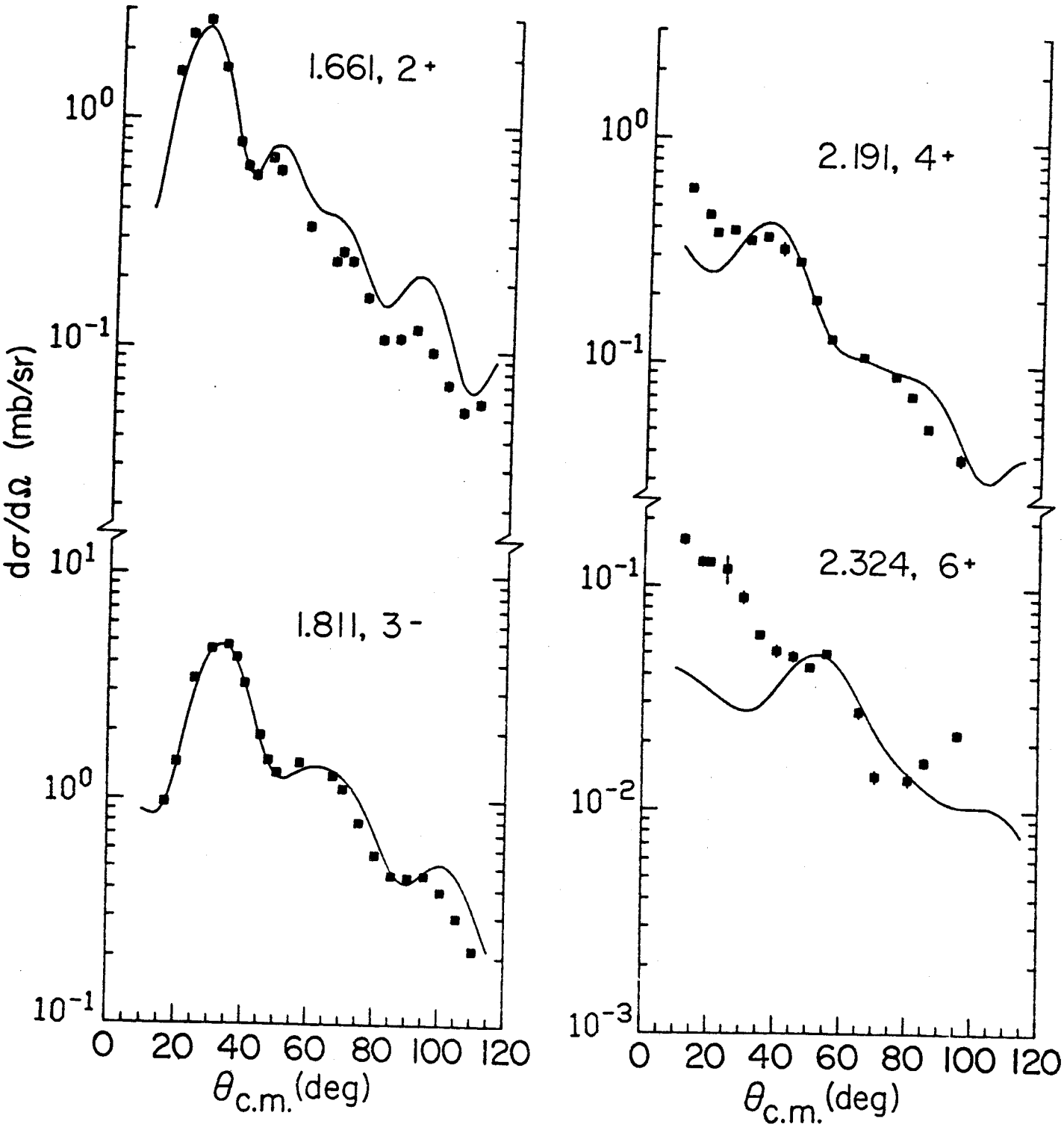
1.661, 2+
1.811, 3-
2.191, 4+
2.324, 6+
dσ/dΩ (mb/sr)
θc.m.(deg)
θc.m.(deg)

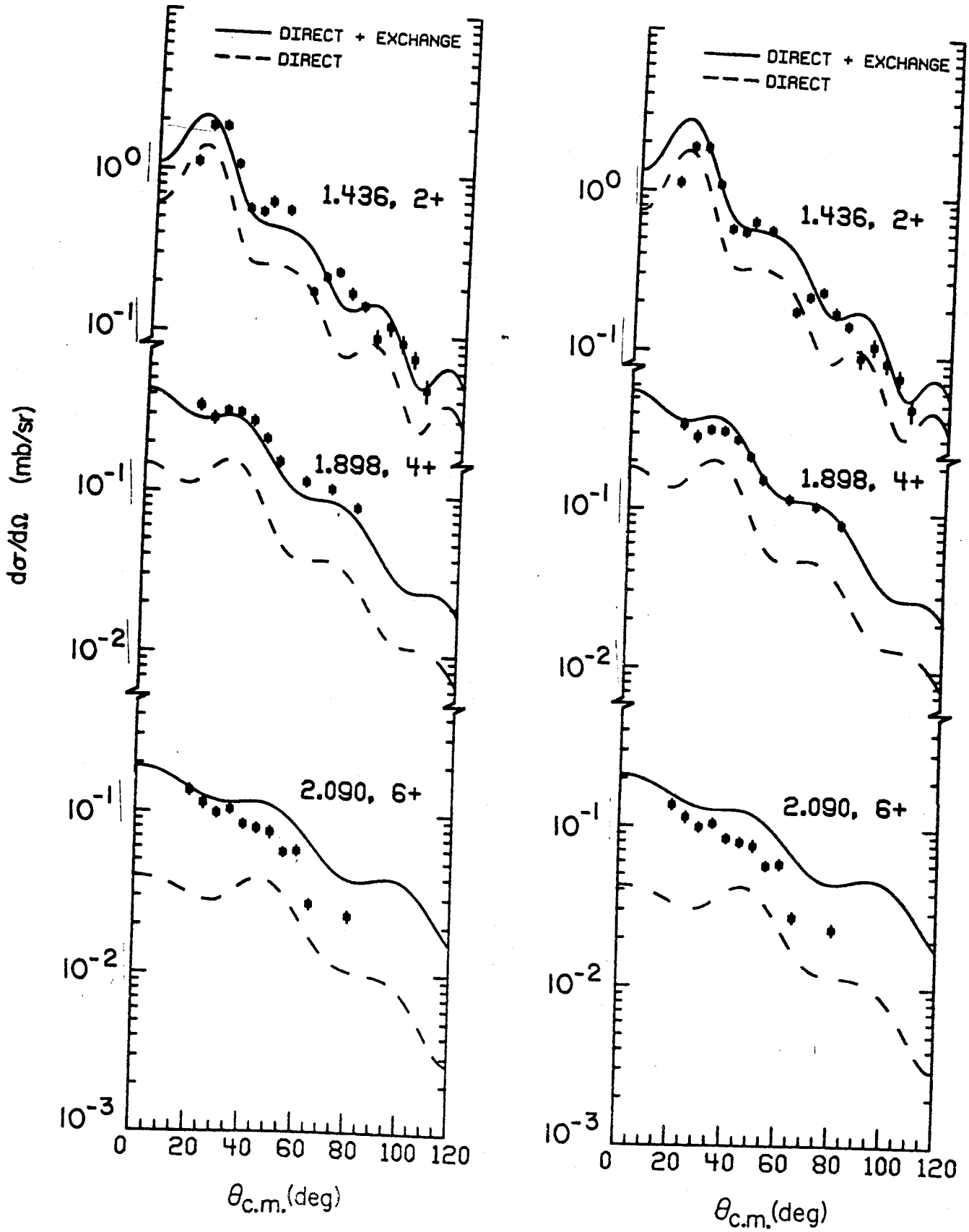
DIRECT + EXCHANGE
DIRECT
1.436, 2+
1.898, 4+
2.090, 6+
dσ/dΩ (mb/sr)
θc.m.(deg)
DIRECT + EXCHANGE
DIRECT
1.436, 2+
1.898, 4+
2.090, 6+
θc.m.(deg)

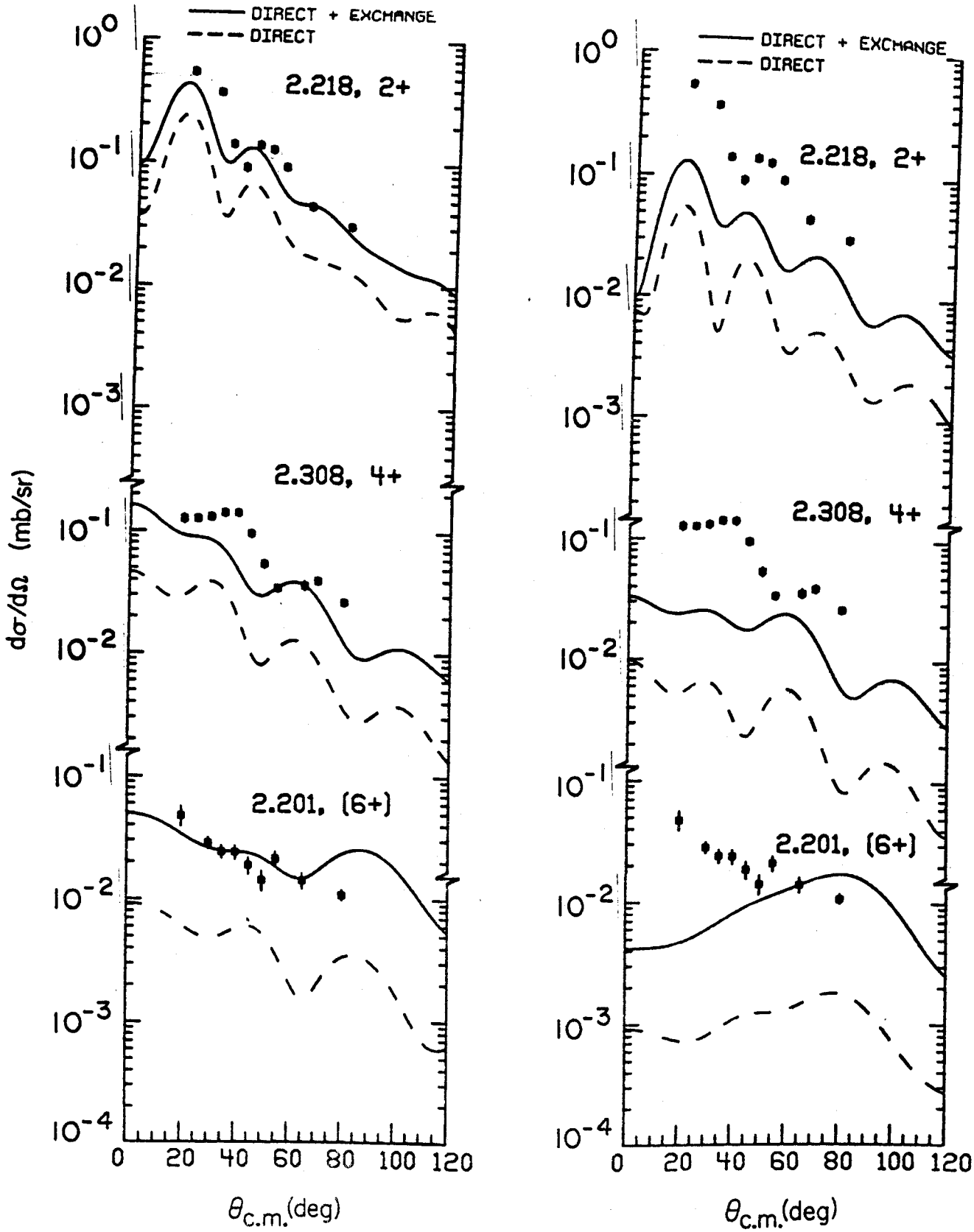
DIRECT + EXCHANGE
DIRECT
2.218, 2+
2.308, 4+
2.201, (6+)
dσ/dΩ (mb/sr)
θc.m.(deg)
DIRECT + EXCHANGE
DIRECT
2.218, 2+
2.308, 4+
2.201, (6+)
θc.m.(deg)

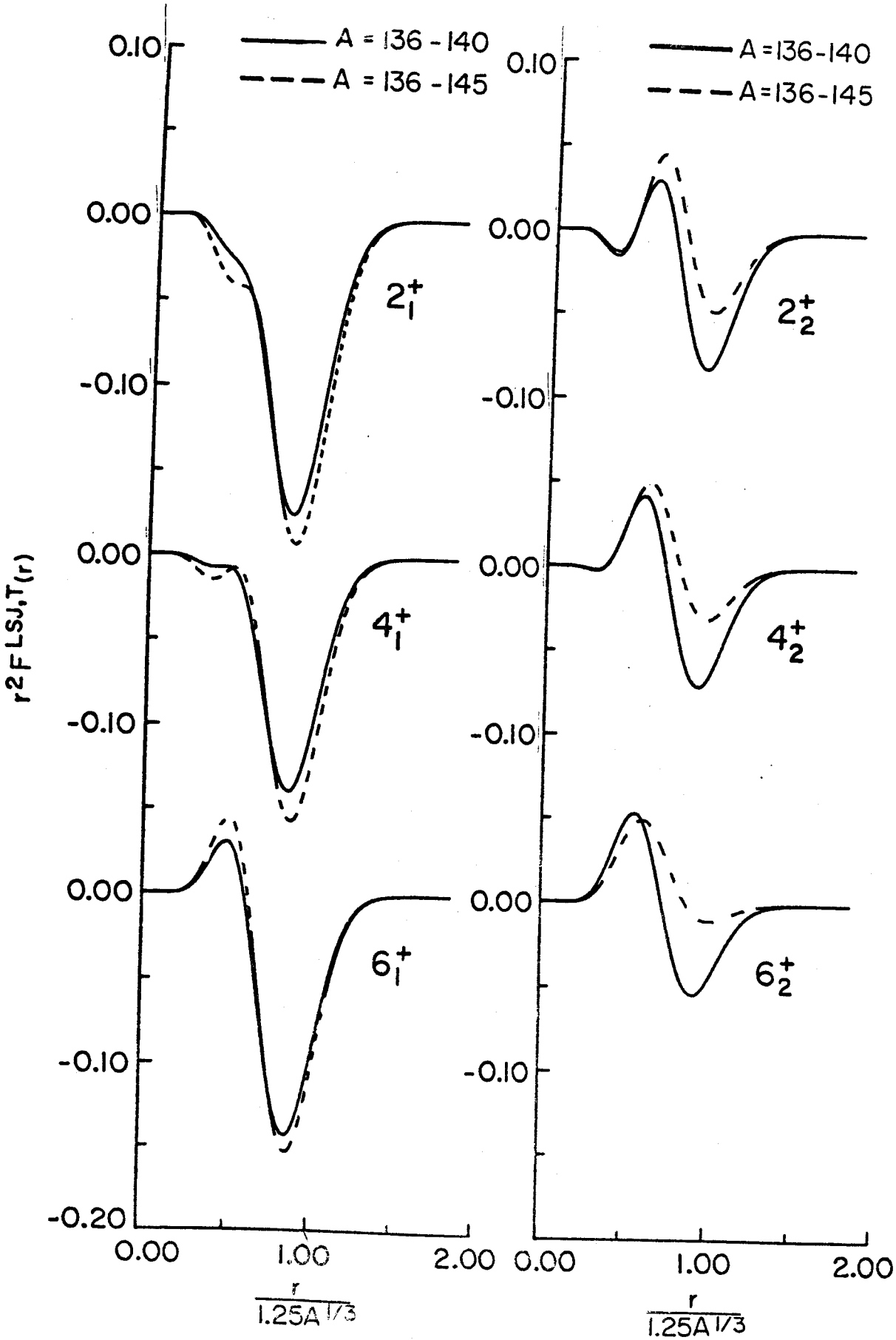
A = 136 - 140
A = 136 - 145
A=136-140
A=136-145
0.10
0.00
-0.10
-0.20
2_1^+
4_1^+
6_1^+
2_2^+
4_2^+
6_2^+
$r^2 F_{LSJ,T(r)}$
0.00
1.00
2.00
$\frac{r}{1.25A^{1/3}}$

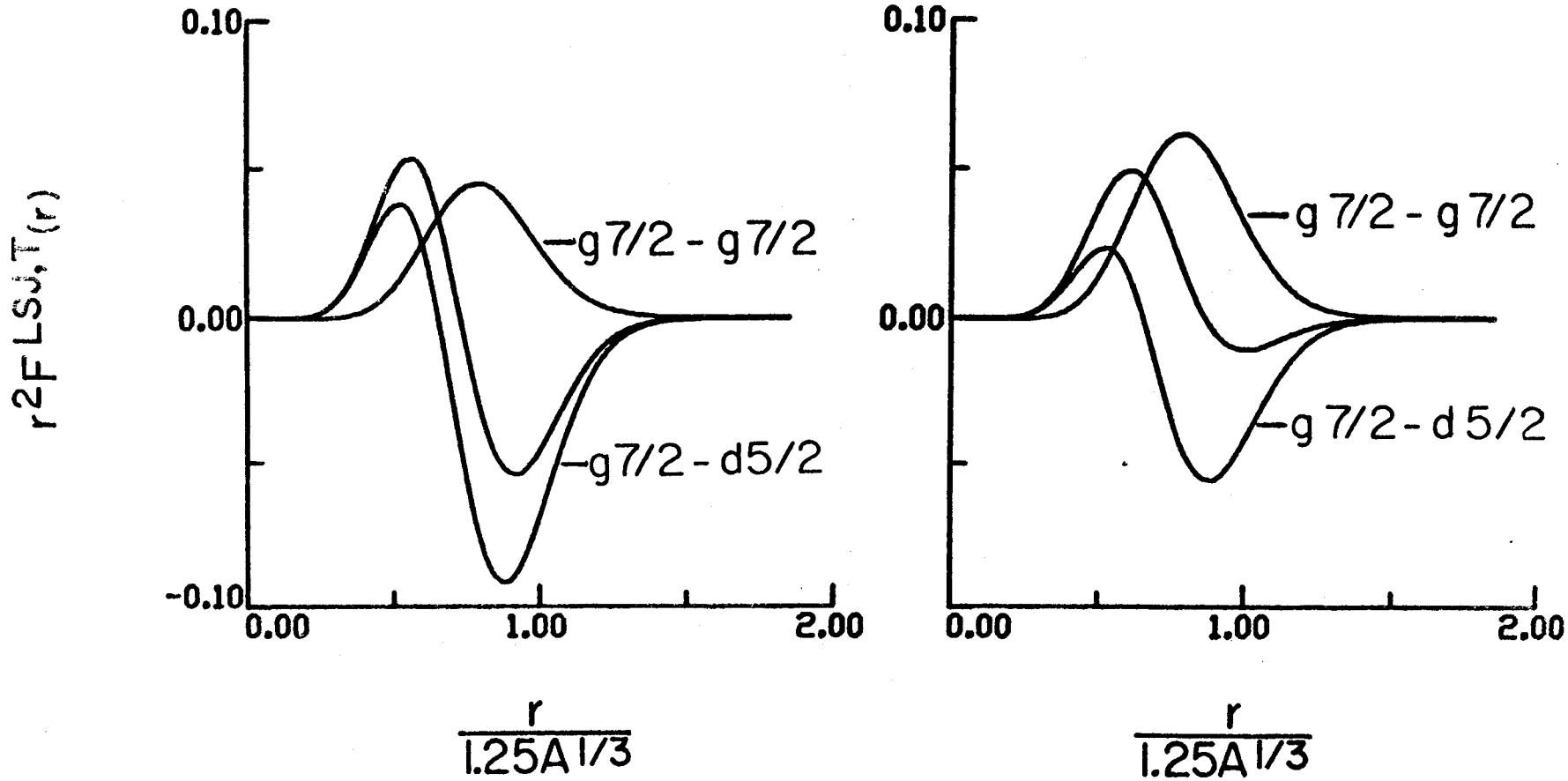
$r^2 F_{LSJT}(r)$
0.10
0.00
-0.10
0.00
1.00
2.00
g7/2 - g7/2
g7/2 - d5/2
$\frac{r}{1.25A^{1/3}}$
0.10
0.00
0.00
1.00
2.00
g 7/2 - g 7/2
g 7/2 - d 5/2
$\frac{r}{1.25A^{1/3}}$

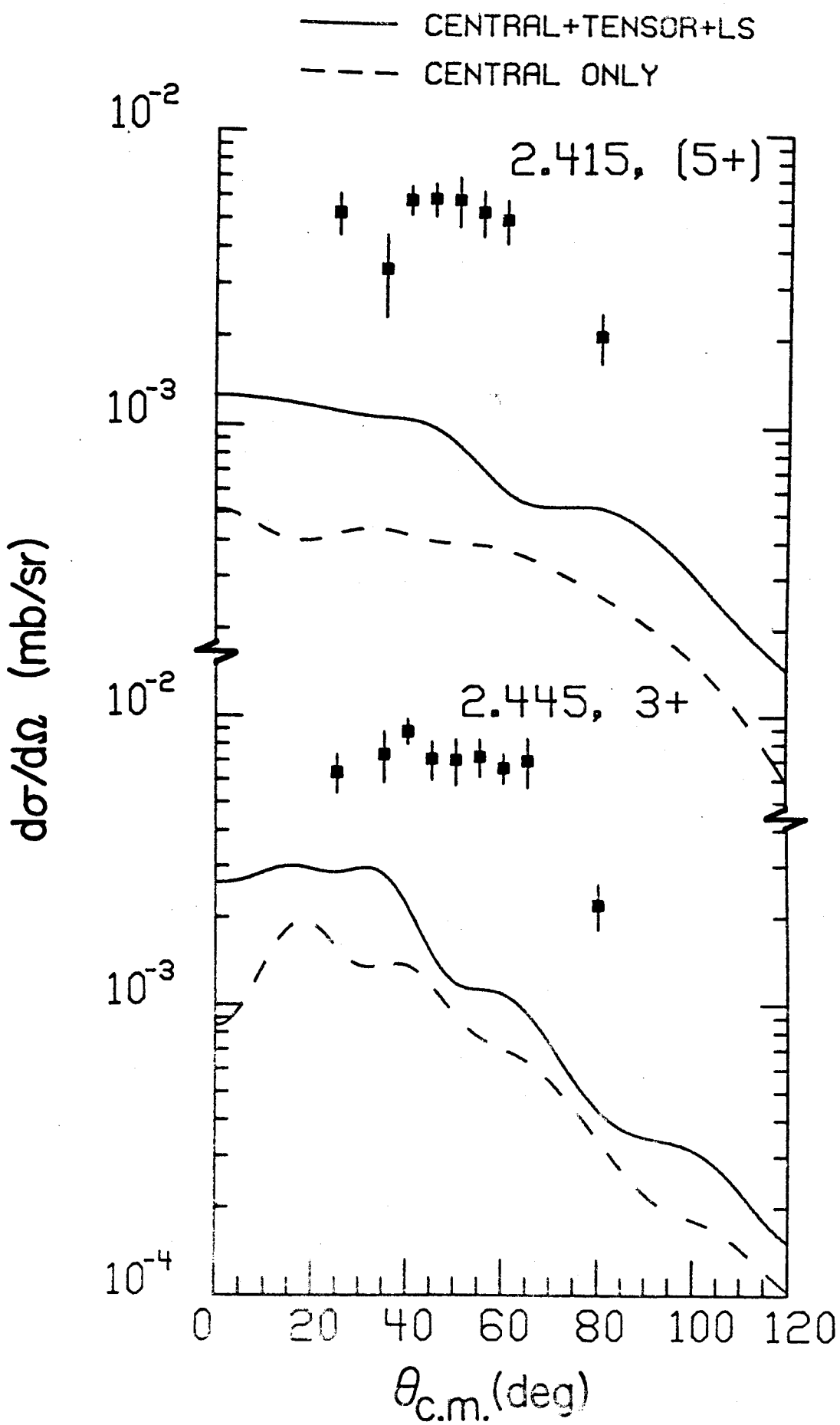
CENTRAL+TENSOR+LS
CENTRAL ONLY
2.415, (5+)
2.445, 3+
dσ/dΩ (mb/sr)
θc.m.(deg)
10-2
10-3
10-2
10-3
10-4
0
20
40
60
80
100
120

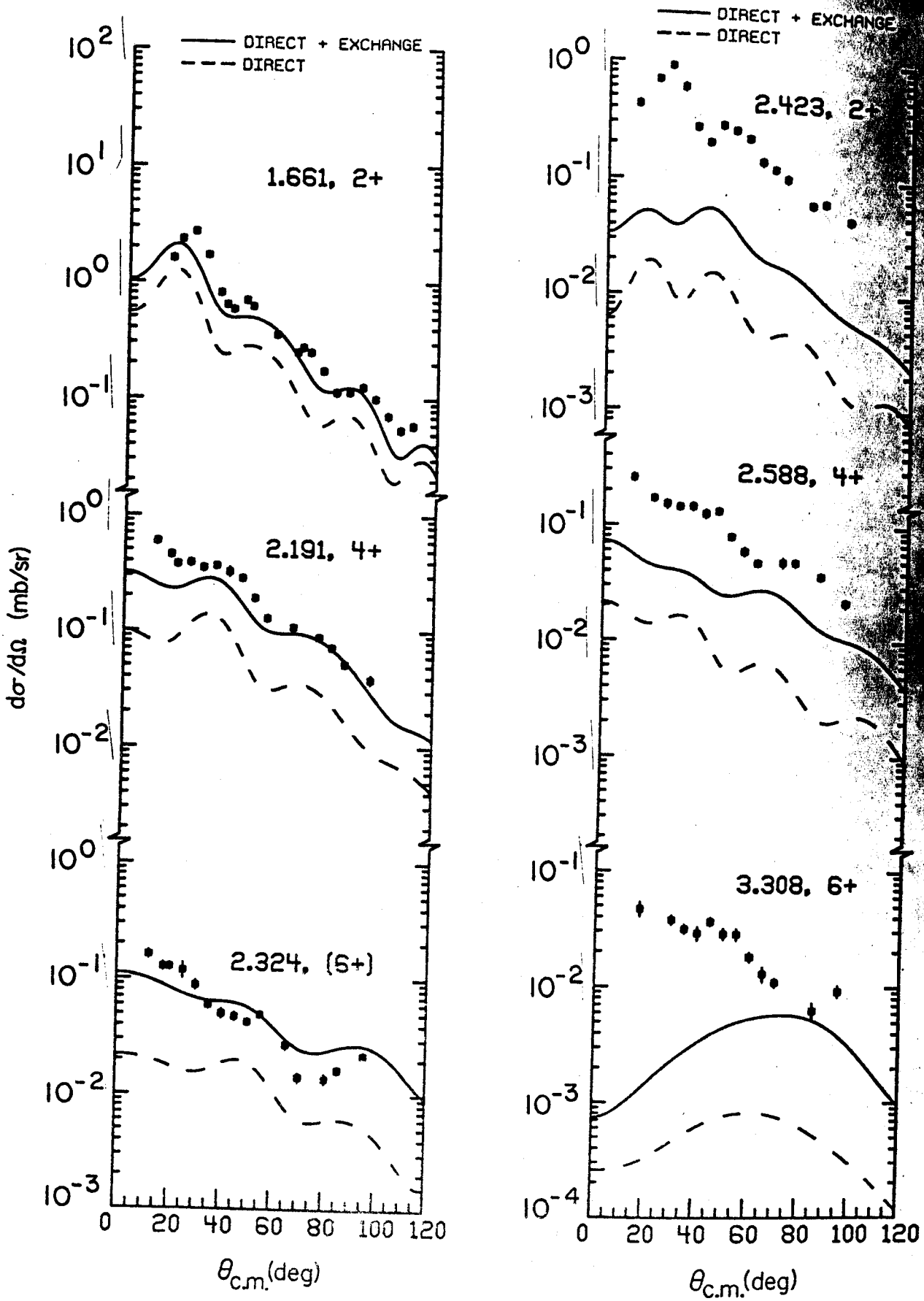
DIRECT + EXCHANGE
DIRECT
1.661, 2+
2.191, 4+
2.324, (5+)
2.423, 2+
2.588, 4+
3.308, 6+
dσ/dΩ (mb/sr)
θc.m.(deg)
θc.m.(deg)